FINITE ELEMENT MODELING OF SYNTHETIC FIBER-ROPES

by

Umut AKALP

B.S., Mechanical Engineering, Boğaziçi University, 2008

Submitted to the Institute for Graduate Studies in
Science and Engineering in partial fulfillment of
the requirements for the degree of
Master of Science

Graduate Program in Mechanical Engineering
Boğaziçi University
2011

dedicated to beloved parents

ACKNOWLEDGEMENTS

Firstly I would like to express my gratitude to my advisor Assist. Prof. Şebnem Özüpek for offering me her full support and encouragement throughout the course of this research, for her patience and time throughout my study.

I would like to convey my gratitude to Prof. Eric B. Becker and Evgeny Podnos for sharing their knowledge with me.

I would like to thank my thesis committee, Assist. Prof. C. Can Aydıner and Prof. Ümit Özgen Çolak.

I would like to thank my friends from graduate studies for their friendships and supports. I am thankful to my officemates for a friendly atmosphere and helpful discussions.

Finally, I would like to thank to my family for their love and support.

ABSTRACT

FINITE ELEMENT MODELING OF SYNTHETIC FIBER-ROPES

The synthetic fiber ropes are used in many fields such as cord fabrics, industrial fabrics, power transmission systems, tires and off-shore applications. The ropes are formed by twisting a small number of yarns which are produced as monofilaments or multi-filaments put together and twisted. Although the use of fiber ropes spread to many fields, there are various challenges related to the characterization and modeling of their mechanical behavior. The main difficulties are associated with the complicated rope structure, the characteristics of the fiber material, contact modeling and determination of friction properties.

Modeling of rope is important because a realistic model would allow the manufacturer as well as the user to be more efficient in designing their products and would reduce the amount of laboratory experiments.

In the study a computational model for twisted yarns and ropes that are composed of many synthetic fibers is developed. In particular two-yarn rope with linear elastic-linear strain hardening material behavior is modeled. The effect of various parameters on mechanical behavior of the rope is investigated through the computational model. Various contact models are investigated and effects of friction, twist level, and initial twist on the axial response of the rope, stress distribution and contact stresses are studied. Results are compared with the results available in the literature.

ÖZET

SENTETİK FİBER İPLERİN SONLU ELEMANLAR METODU İLE MODELLENMESİ

Sentetik lif ipler, kord bezi, endüstriyel bezler, güç iletim sistemleri, lastik ve açık deniz uygulamaları gibi birçok alanda kullanılmaktadır. İpler, bir veya birden çok filamentin oluşturduğu az sayıdaki ipliğin birkaç kat halinde bükülmesiyle oluşur. Sentetik lifli iplerin yaygın kullanım alanlarına karşın, mekanik davranışlarının modellenmesi ve karakterizasyonu ile ilgili birçok zorluk mevcuttur. Başlıca zorluklar ipin karmaşık yapısı, lif malzemesinin özellikleri, temas modellemesi ve sürtünme özelliklerinin belirlenmesidir.

İplerin mekanik davranışının gerçekçi modellenmesi gerek üreticinin gerekse kullanıcının kendi ürünlerini daha etkin olarak tasarlamasını sağlayacak ve laboratuar deneylerinin sayısını azaltacaktır.

Bu çalışmada çok sayıda sentetik liften oluşan iplikler ve bükümlü ipler için hesaplamalı bir model geliştirilmiştir. İki katlı ip, doğrusal elastik-doğrusal gerinim sertleşmesi gösteren malzeme davranışı ile modellenmiştir. Çeşitli parametrelerin ipin mekanik davranışı üzerindeki etkisi hesaplamalı model kullanılarak incelenmiştir. Çesitli temas modelleri çalışılmış, sürtünmenin, büküm seviyesinin ve ilk bükümün ipin eksenel davranışına olan etkisi, gerilme dağılımı ve temas gerilmeleri belirlenmiştir. Sonuçlar literatürde bulunan değerlerlar ile karsılaştırılmıştır.

TABLE OF CONTENTS

LIST OF FIGURES

LIST OF TABLES

LIST OF SYMBOLS/ABBREVIATIONS

a	Length of contact area
b	Width of contact area
c	Constraint
C	Torsional Stiffness
E	Modulus of Elasticity
f_R	Reaction Force
f^α, f_A^α, f_B^α	Predefined field variables
F_1	Total axial force on central wire
F_2	Total axial force on outer wire
F_{total}	Total axial force on rope
g	Gravity
G	Bending moment on wire cross section in x-direction
G'	Bending moment on wire cross section in y-direction
h	Initial length of rope
$\bar{h}$	Final length of rope
h_c	Distance between mass and rigid surface
H	Twisting moment in wire
H_s	Hardening Modulus
I	Moment of Inertia
k	Spring stiffness
K	External moments per unit length on a helical wire in x-direction
K'	External moments per unit length on a helical wire in y-direction
m	Mass
m_2	Number of outer wires
N	Shearing force on cross section in x-direction
N'	Shearing force on cross section in x-direction
p	Hertzian pressure distribution

p_2	Pitch of outer wire
P_f	Load at Fracture
P_y	Load at yield
r_2	Distance between centers of central wire and outer wire at initial configuration
$\bar{r_2}$	Distance between centers of central wire and outer wire at final configuration
R	Radius of wire
R_1	Radius of central wire
R_2	Radius of outer wire
R_1', R_1'', R_2', R_2''	Principal radii of curvatures
T	Axial tension in wire
u	Displacement of mass
U	Axial displacement
X	External distributed force on a helical wire in x-direction
X_2	Distributed force along the center line of outer wire
X_c	Force per unit length along the contact line
Y	External distributed force on a helical wire in y-direction
Z	External distributed force on a helical wire in z-direction
α_2, $\bar{\alpha_2}$	Helix angle
β_2	Rotational Strain
$\dot{\gamma}$	Slip rate
δ	Differential
Δ	Difference between two values
ϵ	Penalty parameter
ε	Strain
θ_2	Angle of twist
$\bar{\theta}$, θ_A, θ_B	Temperature
Θ	External moments per unit length on a helical wire in z-direction
κ, $\bar{\kappa}$	Normal curvature components

κ', $\bar{\kappa}'$	Binormal curvature component
λ	Lagrange multiplier
μ	Friction coefficient
ν	Poisson's ratio
ξ_1, ξ_2	Strain of central and outer wire
σ	Stress
σ_{xx}, σ_{yy}, σ_{zz}	Principal Stresses
τ	Twist per unit length
τ_s	Twist per unit length of the strand
τ_{max}	Maximum shear stress

C3D8	8-node linear brick element
C3D20	20-node quadratic brick element
FE	Finite Element
FEA	Finite Element Analysis
FEM	Finite Element Method
LSM	Least Square Method

1. INTRODUCTION

The synthetic fibres and cords have many fields of use such as cord fabric, industrial fabrics, ropes, security belts, power transmission systems, tires, hoses and offshore applications. There are many different material types used in manufacturing of cords such as nylon, polyester, polypropylene, polyethylene, aramid and rayon[1]. The main advantages of synthetic-fiber ropes are their low weight and flexibility making them preferred replacement of wire ropes.

These ropes are produced from twisted yarns which consist of monofilaments or multifilaments. Monofilaments are large diameter fibers and their diameter are about $100\mu m$. Multifilaments are assembly of few hundred continuous fibers twisted to obtain a yarn. Yarns are braided together or simply twisted together to obtain cords. Then yarns are twisted in the opposite direction to obtain a cord. Therefore stable rope is obtained which is resistant to untwist.[1] Also twisting is the primary mechanism for binding fibers which allows high flexibility. Twisting also strengthens the yarn up to a point. There are two types of twist namely S or right-handed twist and Z or left handed twist. In this study yarns are S twisted and cord is Z twisted.

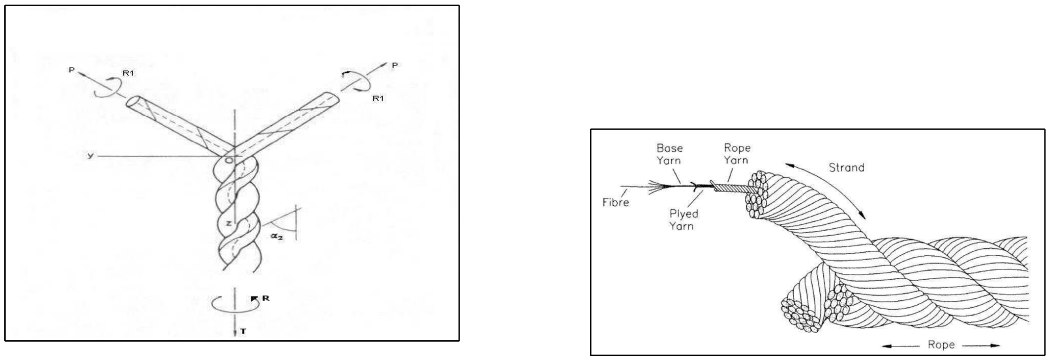

(a) Production of Rope (b) Components of Rope [2]

Figure 1.1. Production of Rope

Figure 1.2. Nylon 66 Tire Cord

Although the use of synthetic-fibers is spreading to many fields, there are various challenges to overcome along the way. Modeling of yarn mechanical behavior is important. The mechanical properties of yarns such as elongation to break, yarn strength, stiffness, and even surface texture effects are dependent on parameters such as twist level, mechanical properties, number of the fiber, and orientation of fibers and interface properties such as friction. Therefore a computational model that predicts the mechanical behavior of the yarns and ropes is desired to evaluate the effect of these parameters. Such a model would allow the manufacturer as well as the user to be more efficient in designing their products and would reduce the amount of laboratory experiments.

The main difficulties are associated with the complex geometry of the ropes and the characteristics of the fiber material. Firstly the fibers in a rope or cord are numerous. They are also variable in length. There is a possibility of variability of the fibre property in a rope. There may be variability of the rope property caused by the production process. Some materials used in rope production have viscoelastic or viscoplastic behavior.

Realistic modeling of ropes should take into account main features stated above and is yet to be developed.

Previous studies can be grouped in three different categories namely; constitutive modeling, computational models, and friction studies.

1.1. Constitutive Models

David A. Zimliki [1] constructed a mathematical model that can predict the properties of flat/twisted yarns and twisted cords from a single filament data. The model is based on a energy method in which work required to stretch a bundle must be equal to the work required to stretch all of the filaments. Model predicts the tenacity elongation to break modulus of twisted cords and shows the effects of twist of filaments into yarns. The assumption made in this study is that yarns consist of continuous fibers. They also neglected the fiber migrations. Model predicts the tenacity, elongation to break, modulus of twisted cords, and shows the effects of twist of the filaments. However it does not predict the effect of contact of yarns and effect of loading during the twist of cord.

E. Chailleux and P.Davies [3] proposed viscoelastic viscoplastic model in order to estimate the tensile behavior of the aramid fiber yarns. The model divides the strain of a fiber into two components namely nonlinear viscoelastic and irreversible plastic. Loading history is taken into account through the viscoelastic model. Plasticity is modeled through a logarithmic law. The model is verified with test data and results are satisfactory. E. Chailleux and P. Davies [4] used their previous model to predict the strain of fibers of ropes under arbitrary loading. They concluded that model is capable to predict mechanical behavior of polyester fibers under random loading sequence. They also suggested that the model can be used as an input to a model which simulates the construction of ropes. However, model does not predict the effect of twist level and fiber/yarn interactions.

D. B. Adolf *et al* [5] constructed analytical model which predicts the mechanical behavior of monofilament nylon fiber. Material clock, the dependence of viscoleastic relaxation rates on thermomechanical history, is a function of potential energy of the system. The study also has experimental part in which monofilament nylon fibers were subjected to numerous tests. Predictions for compression and tensile yield were accurate for different temperatures, enthalpy relaxation, various physical aging tests

and creep. Results showed that, isotropic elastic or viscoelastic material model can be used in order to predict mechanical behavior under uniaxial loading. In other words anisotropic material model can be reduced to isotropic model.

R. D. Averett *et al* [6] investigated the mechanical behavior of nylon 66 fibers under monotonic and cyclic loading. They were interested in fracture process of nylon fibers as well as the stress-strain relationship under monotonic and cyclic loading. They found that monotonic response of nylon 6.6 fibers is best described as linear elastic linear strain hardening. Data found by Averett et al is used as material model in this study.

I. V. Yannas *et al* [7] measured strain recovery and stress relaxation of polyester and nylon 6.6 filaments under two types of temperature history. Below the glass transition temperature ($T_g \simeq 80^oC$) material becomes stiff and springy because the relaxation times becomes longer.

R.H. Blanc and A. Ravasoo [8] determined experimentally the time-dependent stress relaxation for nylon fibers. They also developed a nonlinear model for the stress relaxation. The model is valid for small strain domain and uses modified equation of the quasi linear viscoelastic theory. They observed that stress decayed exponentially with time. The non-linear model has good accuracy and is consistent with experimental data.

1.2. Computational Models

Joe Padovan's [9] study is for cord reinforced composites and takes rubber cord matrix into account. Twist level is included as a parameter in this model so that coupled forces can be applied. Since emphasis is given to elastomeric materials, large deformation formulation is used with thermo-elastic law for cord-reinforced composites. Verification is done by comparing the results with FE Analysis. Model and FE Analysis are consistent and good correlation is achieved. However study does not include rubber-cord interaction or cord-cord interaction. J. Padovan's another study [10] investigates the cord-rubber interface in which interaction modeling is a part of the model. Results show that critical interfacial shear stresses reside at the cord ends for

long cords.

R. M. V. Pidaparti and A. W. May [11] built 2D and 3D FE models for cord-rubber composites. Results are compared with experimental data and other FE results available in literature. In all models they used quadratic elements. In their trials they also used mixed formulation elements. Although cords are assumed as linear isotropic materials, they suggested that for realistic model cord anisotropy should be included. They investigated interface stresses and effect of twisting. To investigate the effect of twisting they differentiate the effective cord modulus. The predicted effective composite properties are comparable to the experimental data.

R. M. Pidaparti et al [12] investigated the interface stresses of cord-rubber structure. Their aim was to study the effect of cord shape on load transfer mechanism. They used 3D models and linear elastic behavior for the properties for the cord. Four different elastic moduli were used for rubber matrix in order to determine the effect of rubber modulus on interface stresses. Twisted cords gave interface stresses 80% higher than the untwisted cords.

O. H. Yeoh [13] studied some benchmark problems by using FEA. Objective was to investigate the effects of different element types, material models, bulk moduli and specimen geometry-aspect ratio. Main benchmark problem studied was torsion of a rubber cylinder. 2-D and 3-D elements as well as displacement or mixed displacement-pressure formulation were used. Neo-Hookean and Mooney material models for hyper elastic materials were considered. Results showed that 2-D axisymmetric models are more efficient and accurate. Study also showed that reaction moment due to twist is independent of bulk modulus for both material models. 3-D quadratic elements gave better results than 3-D linear elements for this specific problem.

1.3. Friction Studies

C. M. Leech [14] studied modeling of synthetic ropes. The geometry was assumed to be hierarchically composed of fiber, yarn, strand and rope. Strains at each level were connected to lower and higher levels through a geometric parameter. The fibers were assumed to be effective only in axial loading. In this study the total virtual

work principle was applied which is advantageous for multi-component systems. The total strain energy was computed by summation over all layers. The external work was calculated for the extension and twist of one rope end with respect to the other under axial load and torque. In a later work Leech [2] calculated the contact forces between the components. In particular six different modes of friction were defined: linear sliding, twist slip, sawing and scissoring between components and distortion and dilation within components.

Literature review shows that there are material models of synthetic fibers and computational models of fiber reinforced components. However there is no computational model for the synthetic fibres and cords which simulates to the production process.

This study aims to develop computational model for twisted yarns and ropes that are composed of many synthetic fibers. Objectives are to investigate the effect of various parameters on the mechanical behavior of ropes through a realistic finite element model. The study includes various models for a rope composed of two yarns twisted together.

Models are in 3-D in order to investigate the effect of friction on strength of cord structure. The effect of production process is studied by applying different loadings.

In Chapter 2 analytical approach found in the literature is reviewed. Formulation of the axial response and contact stress is given in this chapter. Chapter 3 contains the background theory for contact mechanics. The contact formulation used in analytical approach is explained in details. The computational contact mechanics for this approach, which is known as Hertzian Contact, is also presented. Chapter 4 includes the finite element modeling of a two-ply rope. Several models are presented and the effect of various parameters on the axial behavior of the rope are discussed. The results are presented in Chapter 5 and some comparison with the analytical models are given. Conclusion and discussion are presented in Chapter 6.

2. ANALYTICAL APPROACHES

Costello constructed an analytical model predicting the mechanical behavior of wire ropes [15].The geometry consists of a straight central wire surrounded by outer helical wires. Based on this formulation mechanical response of a rope can be calculated for small deformations and linearly elastic isotropic materials. Costello also proposed a formulation for contact forces between wires which is based on Hertz contact problem. In the following a summary of Costello's analytical model is presented.

2.1. Axial Response of Rope

Forces and moments on the helical wire are shown in the Figures 2.1 and Figure 2.2.

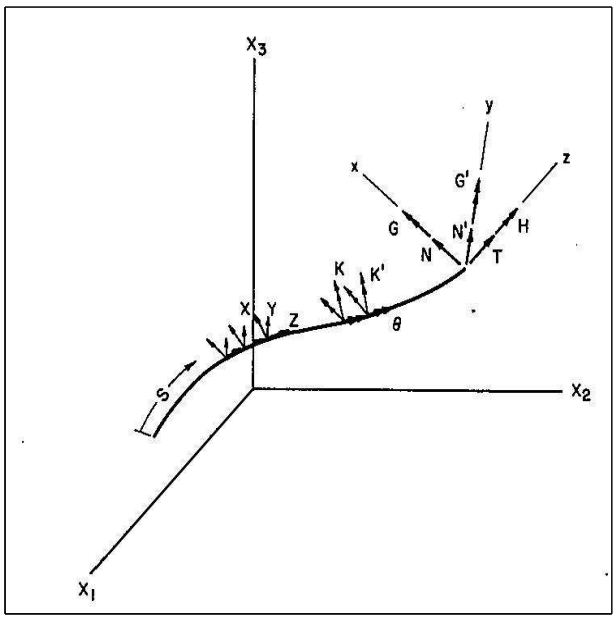

Figure 2.1. Forces on a helical wire [15]

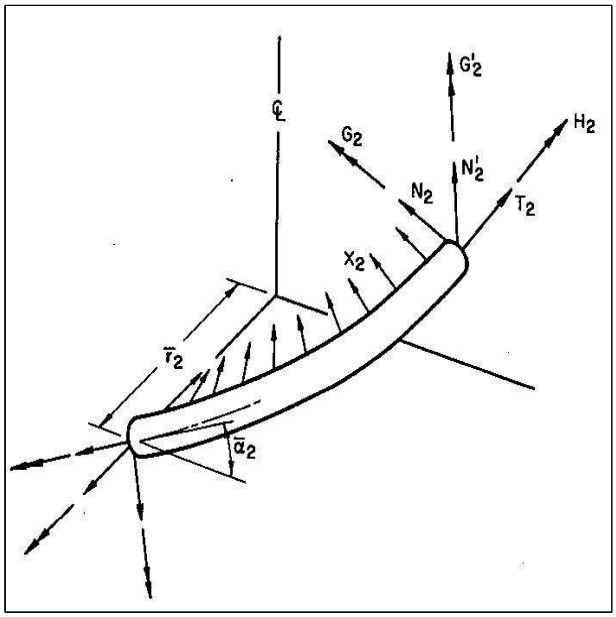

Figure 2.2. Forces on a wire under tension loading [15]

Table 2.1. Forces on a helical wire

X,Y *and* Z	external distributed forces
K, K' *and* Θ	external moments
G *and* G'	bending moments on wire cross section
H	twisting moment in wire
N *and* N'	shearing force on cross section
T	axial tension in wire
τ	twist per unit length
κ *and* κ'	normal and binormal curvature components

For the outer wire equations for force equilibrium are;

$$\begin{aligned} \frac{dN}{ds} - N'\tau + T\kappa' + X = 0 \\ \frac{dN'}{ds} - T\kappa + N\tau + Y = 0 \\ \frac{dT}{ds} - N\kappa' + N'\kappa + Z = 0 \end{aligned} \tag{2.1}$$

and equations for moment equilibrium are;

$$\begin{aligned} &\frac{dG}{ds} - G'\tau + H\kappa' - N' + K = 0 \\ &\frac{dG'}{ds} - H\kappa + G\tau + N + K' = 0 \\ &\frac{dH}{ds} - G\kappa' + G'\kappa + \Theta = 0 \end{aligned} \tag{2.2}$$

In the case of axial loading these six equations become for outer wire;

$$\begin{aligned} &-N_2'\bar{\tau_2} + T_2\bar{\kappa_2}' + X_2 = 0 \\ &-G_2'\bar{\tau_2} + H_2\bar{\kappa_2}' - N_2' = 0 \end{aligned} \tag{2.3}$$

and $Y_2 = 0$, $Z_2 = 0$, $N_2 = 0$, $\Theta_2 = 0$ and since it is assumed that no external bending moment is applied K_2 and K_2' become zero. Subscript "2" in Equations 2.3 indicates that these components are for outer wires.

The relations between changes in parameter τ, κ' and H, G' are;

$$\begin{aligned} &G' = EI_y(\kappa' - \bar{\kappa'}) \quad I_y = \frac{\pi R^4}{4} \\ &H = C(\tau - \bar{\tau}) \quad C = \frac{E\pi R^4}{4(1+\nu)} \end{aligned} \tag{2.4}$$

where C is torsional stiffness, E is elastic modulus, I is the moment of inertia and ν is Poisson's ratio. Note that the cross section of wire assumed as circular.

The strain of central wire under a known axial displacement can be found and therefore the axial strain at outer wire can be found. The relationships between displacement and strains of central ξ_1 and outer wires ξ_2 are;

$$\frac{\bar{h} - h}{h} = \xi_1 = (1 + \xi_2)\frac{sin(\bar{\alpha_2})}{sin(\alpha_2)} - 1 \tag{2.5}$$

where α_2 is the helix angle at initial state $\bar{\alpha_2}$ is the helix angle at deformed state and h and $\bar{h}$ are initial and final length of rope, as seen in Figure 2.3.

Since the deformation is assumed to be small, the change in helix angle is small.

Therefore;

$$\xi_1 = \xi_2 + \frac{\Delta\alpha_2}{tan(\alpha_2)} \tag{2.6}$$

The rotational strain of outer wire is equal to;

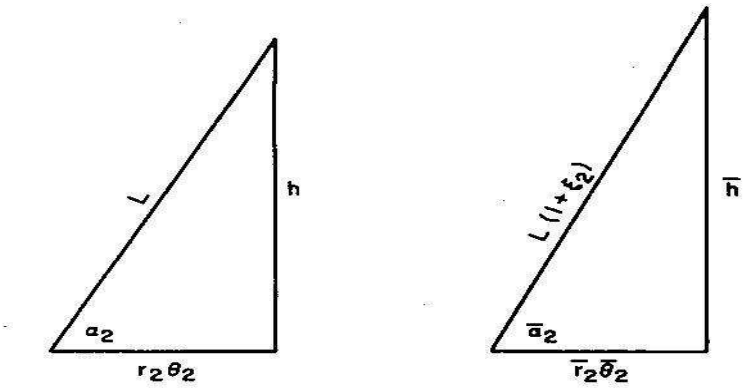

Figure 2.3. Initial and final length of outer wire [15]

$$\beta_2 = r_2\tau_s = \frac{r_2}{\bar{r_2}}\left[\frac{1+\xi_2}{tan(\alpha_2)} - \Delta\alpha_2\right] - \frac{1}{tan(\alpha_2)} \tag{2.7}$$

Since it is assumed that there is no rotational strain, (ie. rotation is constrained) these two equations can be solved together in order to find the change in helix angle, $\Delta\alpha_2$, and strain of outer wire, ξ_2. Once the strain of outer wire and helix angle are found, the forces on the outer wire can be found from the equilibrium equations and from the Equations 2.4. The resulting equations are;

$$\frac{G'_2}{ER_2^3} = \frac{\pi}{4}R_2\Delta\kappa'_2 \tag{2.8}$$

$$\frac{H_2}{ER_2^3} = \frac{\pi}{4(1+\nu)}R_2\Delta\tau_2 \tag{2.9}$$

$$\frac{N_2'}{ER_2^2} = \frac{H_2}{ER_2^3}\frac{cos^2(\alpha_2)}{r_2/R_2} - \frac{G_2'}{ER_2^3}\frac{sin(\alpha_2)cos(\alpha_2)}{r_2/R_2} \tag{2.10}$$

$$\frac{T_2}{ER_2^2} = \pi\xi_2 \tag{2.11}$$

$$\frac{X_2}{ER_2} = \frac{N_2'}{ER_2^2}\frac{sin(\alpha_2)cos(\alpha_2)}{r_2/R_2} - \frac{T_2}{ER_2^2}\frac{cos^2(\alpha_2)}{r_2/R_2} \tag{2.12}$$

where R_2 is the radius of outer wire and r_2 is the distance between the centers of outer wire and central wire.

The projections of these forces on axial direction of strand must be found in order to calculate total axial force on strand. The sum of these projections are;

$$F_2 = m_2(T_2 sin(\alpha_2) + N_2' cos(\alpha_2)) \tag{2.13}$$

where m_2 is the number of outer wires. In the case of two ply cord this value will be 1. Total axial force on central wire can be calculated by using the stress-strain relation;

$$F_1 = ER_1^2\pi\xi_1 \tag{2.14}$$

Finally total axial force is equal to;

$$F_{total} = F_1 + F_2 \tag{2.15}$$

F_{total} is the total reaction force found by this approach. The FE results are compared with this quantity in this study.

2.2. Contact Stresses

Costello also proposed a formulation for contact stresses which is based on Hertz Contact Theory. The distributed force applied on outer wire is the force which causes contact stresses. This force "X_2" is the force per unit length along the centerline of outer wire. Therefore it must be converted to force per unit length along the contact line. This conversion can be done by using the equation;

$$X_c\sqrt{p_2^2+(2\pi R_1)^2}=X_2\sqrt{p_2^2+[2\pi(R_1+R_2)]^2} \tag{2.16}$$

where p_2 is pitch of outer wire and is equal to

$$p_2=2\pi r_2\tan(\alpha_2) \tag{2.17}$$

Based on Hertzian Contact Theory, when two cylinders are contact along their axes of symmetry, the contact surface becomes a narrow rectangle [16]. When $\frac{b}{a}$, the ratio of semiminor axes of the contact area, becomes zero the expressions for stresses at points below the contact surface do not involve elliptic functions. Therefore principal stresses are

$$\sigma_{yy}=-2\nu\left[\sqrt{1+\left(\frac{z}{b}\right)^2}-\frac{z}{b}\right]\frac{b}{\Lambda} \tag{2.18}$$

$$\sigma_{xx}=-\left[\frac{(\sqrt{1+(z/b)^2}-z/b)^2}{\sqrt{1+(z/b)^2}}\right]\frac{b}{\Lambda} \tag{2.19}$$

$$\sigma_{zz}=-\left[\frac{1}{\sqrt{1+(z+b)^2}}\right]\frac{b}{\Lambda} \tag{2.20}$$

Note that when ratio $\frac{b}{a}$ is zero the contact surface is a line and no excessive deformation occurs at contact surface. The principal stresses are maximum at the contact line. Therefore principal stresses become;

$$\sigma_{xx} = -\frac{b}{\Lambda} \tag{2.21}$$

$$\sigma_{yy} = -2\nu\left(\frac{b}{\Lambda}\right) \tag{2.22}$$

$$\sigma_{zz} = -\frac{b}{\Lambda} \tag{2.23}$$

where

$$b = \sqrt{2X_c\Lambda/\pi} \tag{2.24}$$

and

$$\Lambda = \frac{1}{(1/2R_1) + (1/2R_2)}\left(\frac{1-\nu_1^2}{E_1} + \frac{1-\nu_2^2}{E_2}\right) \tag{2.25}$$

For the contact of two wires or fibers is the case, equation 2.25 becomes [15];

$$\Lambda = \frac{4(1-\nu^2)}{\left[\frac{1}{\rho_1} + \frac{1}{R_2}\right]E} \tag{2.26}$$

since the elastic modulus and Poisson's ratio of the wire is the same. Also note that the radius of curvature of the central wire is equal to $\rho_1 = \frac{R_1}{sin^2(\alpha_2)}$ which indicates that cross section of the central wire under axial loading becomes ellipse.

Maximum shear stress due to contact occurs at the point where the ratio of depth of the point from the surface to the semiminor axis "b"(i.e. relative depth) becomes

$z_s/b = 0.7861$ [16]. At this point maximum shear stress is equal to

$$\tau_{max} = \frac{1}{2}(\sigma_{xx} - \sigma_{zz}) = 0.3\left(\frac{b}{\Lambda}\right) \tag{2.27}$$

The contact stresses versus axial displacement curves found in Equation 2.23 formulation is shown below. It is observed that contact stresses are higher for higher twist level.

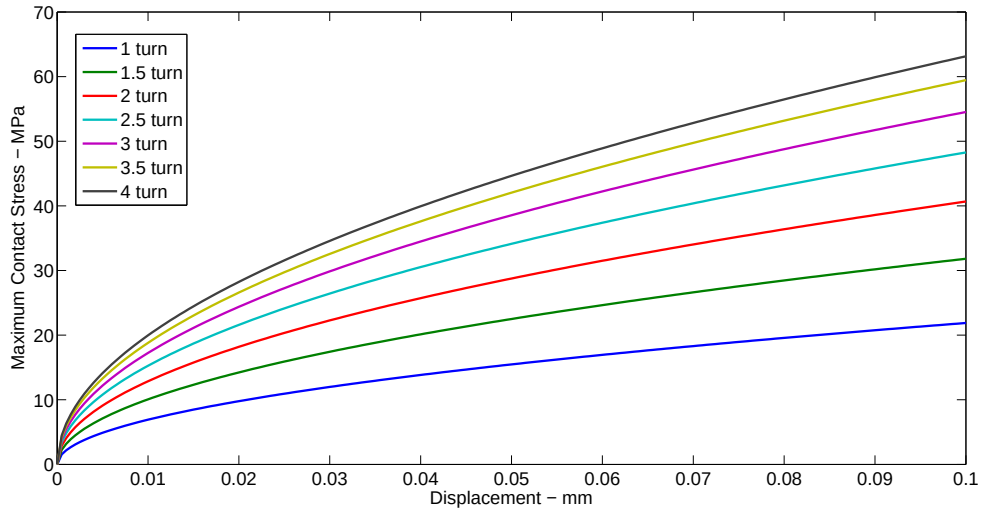

Figure 2.4. U vs Contact Pressure - Analytical results for various number of turns

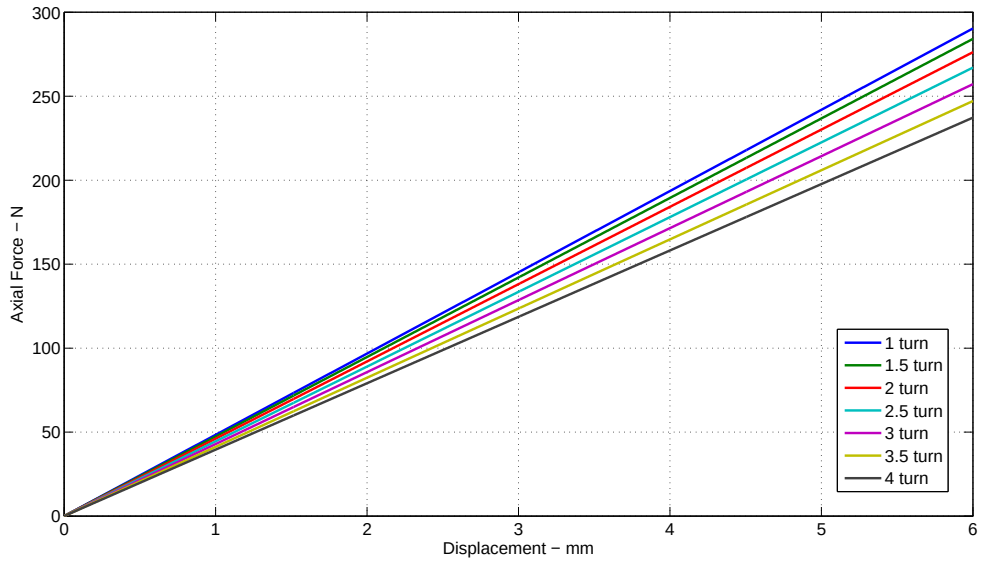

Figure 2.5. U vs Axial Force - Analytical results for various number of turns

3. CONTACT BACKGROUND

3.1. Hertzian Contact

Contact Mechanics requires to predict the shape of the contact area and the relation between the size of area and load [17][18]. It is also required to predict the magnitude and distribution of surface tractions. Hertzian theory assumes that contact surfaces are smooth on both micro and macro scale. Consider the contact of two bodies with curved surfaces. Initial distance between contact surfaces can be defined in the form of;

$$h(x, y) = Ax^2 + By^2 + Cxy \tag{3.1}$$

where $h(x, y)$ is also equal to the difference between the profiles of two surfaces.

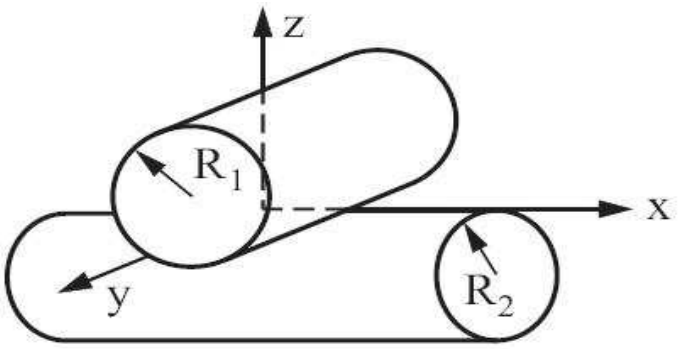

Figure 3.1. Configuration of two cylinders in contact [18]

Hertzian contact theory made second assumption here. According to the theory, contact occurs on a plane which is chosen as z-plane in Figure 3.1. In order to make the formulation simple the origin is chosen as the first point of contact and axes are chosen such that coefficient C vanishes. In general, the profiles of two surfaces can be written as;

$$z_1 = \frac{1}{2R_1'}x_1^2 + \frac{1}{2R_1''}y_1^2 \quad and \quad z_2 = \frac{1}{2R_2'}x_2^2 + \frac{1}{2R_2''}y_2^2 \tag{3.2}$$

The terms R'_1, R''_1, R'_2 and R''_2 are the principal relative radii of curvatures of the surfaces. The constants A and B in Equation 3.1 can be found from the following equations:

$$A + B = \frac{1}{2}\left(\frac{1}{R'_1} + \frac{1}{R''_1} + \frac{1}{R'_2} + \frac{1}{R''_2}\right) \tag{3.3}$$

$$(A - B)^2 = \frac{1}{2}\left[\left(\frac{1}{R'_1} - \frac{1}{R''_1}\right)^2 + \left(\frac{1}{R'_2} - \frac{1}{R''_2}\right)^2 + 2\left(\frac{1}{R'_1} - \frac{1}{R''_1}\right)\left(\frac{1}{R'_2} - \frac{1}{R''_2}\right) cos(2\alpha)\right] \tag{3.4}$$

Note that α is the angle between the principal radii of two surfaces. Therefore this formulation is valid for contact problem of two cylinders at any angle, including α_2 which is the helix angle of a two ply cord introduced in Chapter 2.
For contact of two cylinders which have equal diameters $R'_1 = R'_2 = R$ and $R''_1 = R''_2 = \infty$. There are three different shape of contact area in that case;

- If the axes are perpendicular then the area will be circular
- If two axes are parallel then the area will be narrow rectangle
- If two axes makes an angle different than 0 and 90 degree, then the area will be elliptical.

The pressure distribution proposed by Hertz is;

$$p = p_0\left[1 - \left(\frac{x}{a}\right)^2 - \left(\frac{y}{b}\right)^2\right] \tag{3.5}$$

The pressure defined in Equation 3.5 will produce a displacement within the contact region. This displacement field will be elliptical function and defined in intervals $-b \leq x \leq b$ and $-a \leq y \leq a$.

The displacement field of the surface can be calculated with respect to a reference point which is below the contact surface where no deformation occurs. The displacement function which is elliptical is not defined at that point. The displacement for

both bodies is equal to;

$$\bar{u}_{z1} + \bar{u}_{z2} = \delta - h(x, y) \tag{3.6}$$

where δ is equal to the displacement in the z-direction of a point out of contact region. The assumptions of Hertzian Contact can be summarized as;

- Contact surfaces are continuous (ie. no irregularities) and non-conforming
- The strains and displacements are small
- The width of the contact surface is small compared to radius of the surfaces, so that both of the bodies can be considered as elastic half space
- The surfaces are frictionless, and therefore, there is no tangential surface traction.

3.2. Methodology of Computational Contact Mechanics

1D contact problem is considered to summarize various computational contact models. The problem which consists of a point mass m and a spring with stiffness k[19]. The contact can occur between point mass and a rigid surface which are initially at distance h one from another. The total energy for this spring-mass system is;

$$\Pi(u) = \frac{1}{2}ku^2 - mgu \tag{3.7}$$

where u is displacement of masss m First and second variation of Equation 3.7 give

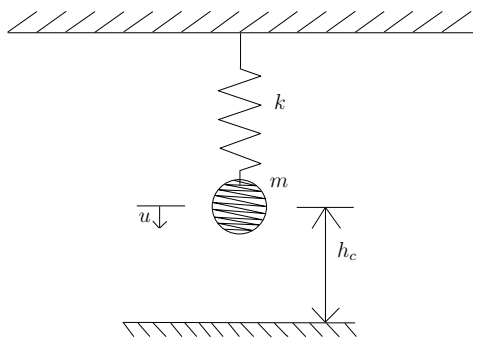

Figure 3.2. 1-D Contact Problem - Spring-Mass System

$$\delta\Pi(u) = ku\delta u - mg\delta u = 0 \tag{3.8}$$

$$\delta^2\Pi > 0 \;\Rightarrow\; \Pi_{min}(u) \;\; at \;\; u = \frac{mg}{k} \tag{3.9}$$

The restriction of the displacement of mass by a rigid support can be described by

$$c(u) = h_c - u \geq 0 \tag{3.10}$$

Equation 3.10 is a constraint, and $c(u) > 0$ if there is a gap between wall and point mass and $c(u) = 0$ when there is no gap. Variation of $c(u)$ gives;

$$\delta c(u) = -\delta u \geq 0 \quad \Rightarrow \quad \delta u \leq 0 \tag{3.11}$$

Since mg will be greater than ku in the case of contact;

$$ku\delta u - mg\delta u \geq 0 \tag{3.12}$$

Equation 3.12 is called variational inequality.
In classical contact mechanics $f_R \leq 0$ where f_R is the reaction force.
To conclude there are two cases.
Case 1: The stiffness of the spring is so large that the point mass does not touch the wall.

$$c(u) > 0 \;\; and \;\; f_R = 0 \tag{3.13}$$

Case 2: Point mass comes into contact with the wall

$$c(u) = 0 \;\; and \;\; f_R < 0 \tag{3.14}$$

Finally these conditions become

$$c(u) \geq 0 \ , \quad f_R \leq 0 \ \ and \ \ f_R c(u) = 0 \tag{3.15}$$

which are known as "Hertz-Signorini-Moreu" conditions in contact mechanics.
In the following two commonly used methods in the solution of contact problem will be described

3.2.1. Lagrange Multiplier Method

The Lagrange multiplier method adds a term to the energy of system which contains the constraint [19]. Therefore energy for the system becomes;

$$\Pi(u, \lambda) = \frac{1}{2} k u^2 - mgu + \lambda c(u) \tag{3.16}$$

where λ is a Lagrange multiplier.
By comparing Equation 3.16 with conditions 3.15, it can be seen that λ is equivalent to f_R.
The first variation of energy of the system with respect to u and λ leads to

$$ku\delta u - mg\delta u - \lambda \delta u = 0 \tag{3.17}$$

and

$$c(u)\delta\lambda = 0 \tag{3.18}$$

Equation 3.18 corresponds to Case 2 given in Equation 3.14. Therefore Equation 3.17 can be solved for λ as

$$\lambda = kh_c - mg = f_R \tag{3.19}$$

If λ value satisfies $f_R < 0$ then $u = h_c$, that is mass and rigid surface are in contact. Otherwise, Lagrange multiplier is zero and u is solved from Equation 3.8

3.2.2. Penalty Method

This method adds a penalty term to the energy of the system [19]. Therefore total energy becomes;

$$\Pi(u) = \frac{1}{2}ku^2 - mgu + \frac{1}{2}\epsilon[c(u)]^2 \text{ with } \epsilon > 0 \tag{3.20}$$

where ϵ is penalty parameter and can be interpreted as a spring stiffness which is between mass and rigid surface. First variation of Equation 3.20 leads to;

$$ku\delta u - mg\delta u - \epsilon c(u)\delta u = 0 \tag{3.21}$$

For $c = h_c - u$ solution of Equation 3.21 gives

$$u = \frac{mg + \epsilon h_c}{\epsilon + k} \tag{3.22}$$

Constraint equation becomes;

$$c(u) = h_c - u = \frac{kh_c - mg}{\epsilon + k} \tag{3.23}$$

Since $kh_c \leq mg$ in the case of contact, penetration of point mass into the rigid surface occurs. It is obvious that penetration depends on the penalty parameter.There are two limiting cases:

i. $\epsilon \to \infty \Rightarrow (u - h_c) \to 0$ which means that correct solution can be obtained for very large penalty parameters. In another words when penalty stiffness is very large small penetration occurs.
ii. $\epsilon \to 0$ represents the unconstrained solution and is only valid for inactive constraints. In the case of contact, very small penalty parameter leads to large

penetration.

For penalty formulation $f_R = \lambda = \epsilon c(u)$

$$f_R = \epsilon c(u) = \frac{\epsilon}{k+\epsilon}(kh_c - mg) \tag{3.24}$$

For $\epsilon \to \infty$ Equation 3.24 leads to the correct solution given in Equation 3.19

3.3. Finite Element Modeling of Contact

Finite Element modeling of contact is a difficult problem since adds a strong nonlinearity to the boundary value problem and is typically responsible for convergence difficulties. Given the key role of contact in simulation of rope behavior, an overview of finite element contact modeling is given next. The goal is to present the steps involved in defining contact rather than to a give detailed theory.
Contact modeling used in this study is discussed in detail in section 4.5.

3.3.1. Contact Formulations

In most Finite Element software including the package ABAQUS used in this study, several contact formulations are provided [20]. Each formulation consists of a particular contact discretization, a tracking approach and assignment of master and slave roles to the contacting surfaces.

3.3.1.1. Discretization Methods. Two different contact discretization methods are available in ABAQUS.
Each slave node of a contact interface efficiently interacts with a point of projection on the master surface on the opposite side of the contact interface . Therefore each contact condition consists of a slave node and a group of master nodes. The values of

the master nodes are interpolated to the projection point.

The penetration of slave nodes is restricted whereas it is not restricted for master nodes. In other words only master nodes can penetrate to slave surface. The contact direction depends on the normal of the master surface. Only information needed for slave nodes are the coordinates and the surface area of each node. There is no requirement for defining a node based surface.

Surface-to-Surface contact formulation forces contact conditions in an average sense over a region of slave nodes. The slave nodes are approximately at the center of regions so each contact constraint depends not only on one slave node but also on adjacent slave nodes. Large and undetected penetrations of master nodes into slave surface are prevented with this discretization. The contact direction depends on an average normal of the slave surface in the regions surrounding a slave node.

Generally surface-to-surface discretization gives more accurate stress and pressure results than the node-to-surface discretization if the surface geometry is not complicated. Node-to-surface discretization enforces slave nodes not to penetrate to master surface individually. Therefore forces on slave surface are concentrated at slave nodes. As a result of this spikes and valleys occur in the distribution of pressure across the surface. Surface-to-surface discretization on the other hand enforces slave nodes not to penetrate to master surface in an average sense over a finite region of slave surface. Therefore the stress and pressure distribution is smooth which is more realistic.

3.3.1.2. Tracking Approach. In FE code used in this study, there are two formulations for modeling the interactions between two deformable bodies.

i. Small sliding formulations in which the contacting surfaces can undergo only relatively small sliding. Arbitrary rotation is permitted.
ii. Finite sliding formulation where separation and high slip rates can occur. Arbitrary rotation of the surface may occur and it is not permitted.

In this study finite-sliding tracking approach is the appropriate choice.

3.3.1.3. Choosing Master and Slave Surfaces. In computational contact mechanics the surfaces are assigned master and slave surfaces. The slave surface is the surface that calculations are made and the nodes on this surface are not allowed to penetrate into master surface. On the other hand, the nodes on master surface are allowed to penetrate into slave surface.

Since the calculations are made at nodes on slave surface, it is obvious to choose surface with finer mesh as slave surface.

If the stiffness and mesh density are same on both surfaces the preferred choice is not obvious. Choice of master-slave surface has less effect on the results with surface-to-surface formulation than with node-to-surface formulation.

Based on Newton's third law of motion, contact forces acting on respective surfaces should be equal and opposite in direction. This statement is always satisfied by surface-to-surface contact. However node-to-surface discretization can generate a net moment. This net moment can occur in cases where there is friction between two surfaces.

There are two different types of contact definition used. One of them namely "General Contact" always uses the finite sliding surface to surface contact formulation. Master and slave surfaces are assigned automatically. In the other contact definition "Surface to Surface" surface to surface discretization option is available as well as node to surface option. Also finite or small sliding formulation can be used in this option.

The General Contact algorithm uses a penalty method to enforce active contact constraints by default. Other enforcement methods can be specified as part of surface interaction (i.e. contact property) definition.

3.3.2. Normal Contact Behavior

There are three constraint enforcement methods [20].

- Direct method enforces constraint without any approximation. In other words the pressure-overclosure relation is strictly enforced without use of augmentation iterations. Solution is accurate, however convergence problems can occur in complex problems. This method can be used by defining hard contact as normal behavior.

- The penalty method is a stiff approximation of hard contact. Penalty method approximates hard pressure-overclosure behavior. In this method contact force is proportional to the penetration. The advantages of this method are;
  i. Numerical softening combined with penalty method can lessen over-constraint issues and the number of iterations required becomes less
  ii. The penalty method provides no need for Lagrange multipliers which results improved solver efficiency.

  Penalty method can be divided into two; linear and non-linear.

  In linear Penalty Method penalty stiffness is constant so pressure-overclosure relationship is linear. In linear method program defines a penalty stiffness as 10 times of the stiffness of representative underlying element. Contact penetrations due to default parameters and adjustments do not affect the results in most cases, however these penetrations can sometimes lead to some degree of stress inaccuracy (for instance, with displacement controlled loading and a coarse mesh).

  In Non-linear Penalty Method penalty stiffness increases linearly between regions of constant low initial stiffness and constant high final stiffness. This creates a nonlinear pressure-overclosure relationship. Non-linear penalty method is applied to model by using exponential pressure-overclosure relationship.
- The augmented Lagrange method also uses stiff approximation as the penalty method. Difference is that it also uses augmentation iterations in order to improve the accuracy of the approximation.

  The penalty or augmented Lagrange constraint enforcement methods sometimes provide more efficient solutions (as a result of lower number of overall iterations per analysis) with a small sacrifice in solution accuracy.

3.3.3. Tangential Contact Behavior

Available models are;

- The Classical Coulomb friction model in which friction coefficient can be defined in terms of static and kinetic friction coefficient
- Anisotropic extension of the basic Coulomb friction model
- A softened interface model sticking friction which can be used with explicit solver
- A model that eliminates frictional slip when surfaces are in contact. [20]

3.3.3.1. Coulomb Friction. This model defines a critical shear stress τ_{crit}=μp where p is the contact pressure. If the slave surface is based on nodes contact pressure is equal to the normal force divided by the cross-sectional area at the contact node. By default cross-sectional area is 1.

The basic model is isotropic friction in which μ is the same in all directions. For a 3-D simulation there will be two components of shear stress τ_1 and τ_2. These two stress components are combined in order to find an equivalent shear stress, $\bar{\tau}$, for stick slip calculations.
In the model shear stress limit and elastic slip definitions were not defined by user and default definitions are used.

In order to define this type of friction at least two data point must be provided. These are μ_1 when slip rate is equal to zero and μ_2 when slip rate have a finite value. FE package automatically calculates a third point (μ_∞,$\dot{\gamma}_\infty$). The third point defines the friction coefficient for large slip rates and it is computed according to the equation. By default coefficient of friction is defined as;

$$\mu = \mu(\dot{\gamma_{eq}}, p, \bar{\theta}, \bar{f^{\alpha}}) \tag{3.25}$$

where
$\dot{\gamma_{eq}}$ is the equivalent slip rate
$\bar{\theta} = \frac{1}{2}(\theta_A + \theta_B)$ average contact temperature at contact point

$\bar{f^{\alpha}} = \frac{1}{2}(f_A^{\alpha} + f_B^{\alpha})$ average predefined field variable at contact point
As default μ does not depend on these variables. So the friction model that was used in analysis is

$$\mu = \mu(\dot{\gamma_{eq}}, p, \bar{\theta}, \bar{f^{\alpha}}) = constant \tag{3.26}$$

and

$$\mu = \mu(\dot{\gamma}_{eq}) \tag{3.27}$$

Equation 3.26 is defined in ABAQUS as penalty friction. The second type of friction is shown in Equation 3.27 and called Static-Kinetic Exponentially decaying friction which is a function of slip rate.

4. FINITE ELEMENT MODELING

3D finite element model of a two-ply nylon 66 rope is developed. In the actual production, bundle of fibers is twisted to form a yarn. Each yarn is a bundle of 200 fibers. Then two yarns are twisted in the opposite direction to build the rope. First objective of the study is to evaluate the effect of the bundle twist.

It was observed that upon untwist, the fibers have some permanent deformations. The second objective of the study is to account for this observation through a plastic material model.

Interaction between yarns and fibers plays an important role in the mechanical behavior of the rope. The third objective of the study is to realistically model the contact between the yarns by considering various computational contact models. Contact between fibers is not modeled in the study.

In order to achieve these objectives several FE models were analyzed. In the following, two models that were successfully completed will be discussed. These are:

- Model 1. Initially twisted yarns subjected to axial loading
- Model 2. Twisted geometry subjected to tension loading

Other models will be discussed briefly in last section of this chapter.
FE package ABAQUS was used in all analyses.

4.1. Geometry

It is assumed that 200 fibers are braided together for making a yarn. Diameter of each nylon 66 fiber is 33μm [6]. Yarns are assumed solid with no spacing between fibers, that is cross sectional area of each yarn is equal to the cross sectional area of a single fiber times the number of fibers. So radius of a yarn is taken as 0,229 mm. There are two yarns in the FE models. The length of each yarn is 20 mm. Yarns are placed tangential to one another in the direction of their axis of symmetry, as seen in

Figure 4.1. In the first model, one yarn is longer than the other by about 0.1 mm as seen in Figures 4.2 and 4.3. Yarns are created with their cylindrical axis parallel to z-axis and their cross section on x-y plane.

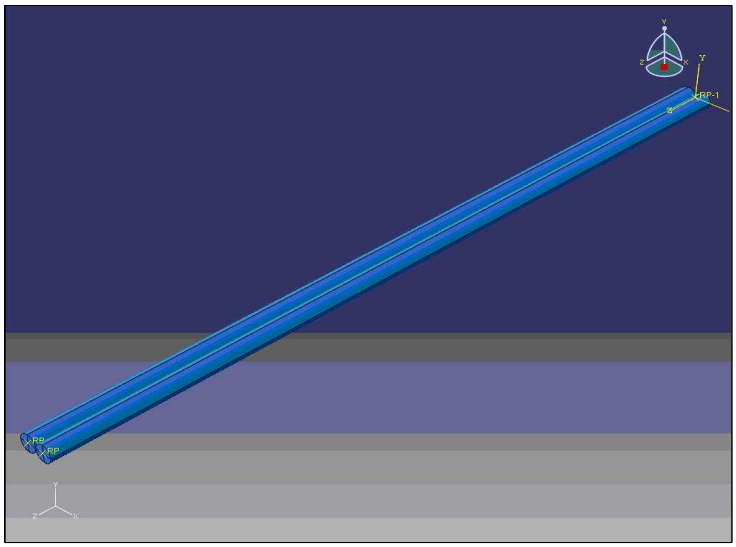

Figure 4.1. Geometry for Model 1

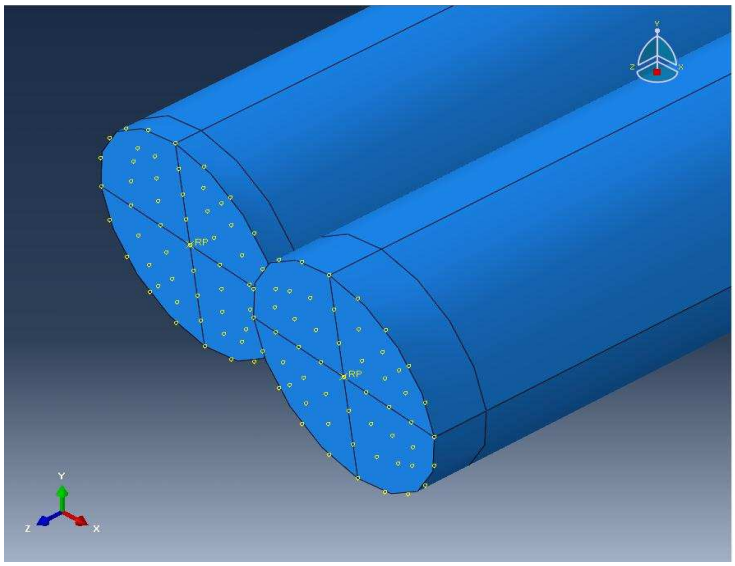

Figure 4.2. End Regions for Model 1 - z=20 mm

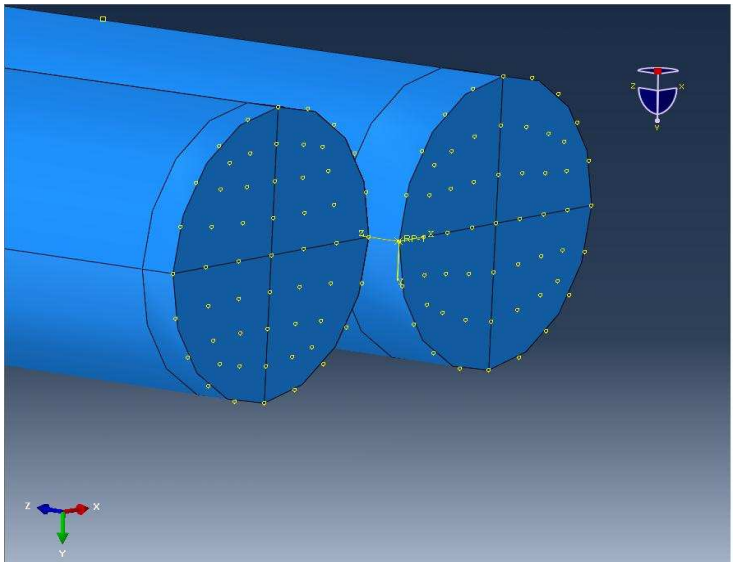

Figure 4.3. End Regions for Model 1 - z=0 mm

In the second model twisted geometry is used for analysis. Model 2 has two parts which are created by using revolution so that twisted geometry is obtained. Twist in this model is equal to the total twist that can be obtain in other models (which is equal to 2.5 turns=900 degrees).

4.2. Material Model

Rope material used in this study is nylon 66. Constitutive behavior of nylon is assumed to have elastic part and plastic part. The model and the data used to calibrate the model are based on work of R. D. Averett [6]. Figure 4.4 shows the load-displacement curve of nylon 66 specimens subjected to uniaxial tensile monotonic load. Properties of 8 nylon 66 fibers determined from tests are given in Table 4.1. Averett *et al* represented the test data through the stress-strain relation

$$\sigma(\epsilon) = \begin{cases} E\epsilon & \epsilon < \epsilon_y \\ \sigma_y + H_s(\epsilon - \frac{\epsilon_y}{E}) & \epsilon \geq \epsilon_y \end{cases} \tag{4.1}$$

where E is Young's modulus and H_s is hardening modulus.

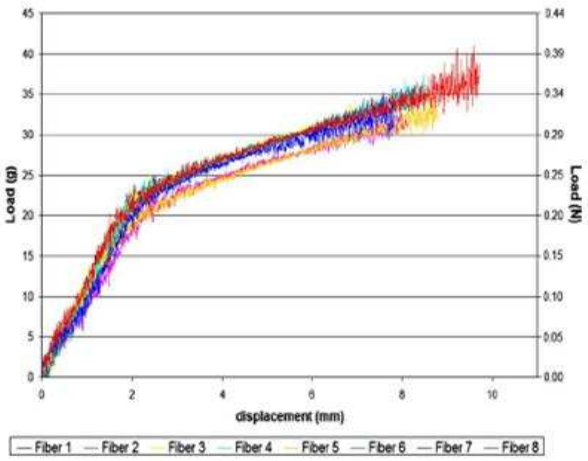

Figure 4.4. Load - Displacement response of nylon 66 fibers [6]

Table 4.1. Test Results for 8 Different Nylon 66 Fibers [6]

$FiberName$	E (GPa)	H_s (MPa)	P_y (N)	P_f (N)	σ_y (MPa)	σ_f (MPa)	ϵ_y	ϵ_f
$Fiber1$	2.9	5.3E+02	0.20	0.34	2.1E+02	3.5E+02	0.07	0.33
$Fiber2$	2.7	4.4E+02	0.17	0.32	1.8E+02	3.3E+02	0.06	0.35
$Fiber3$	2.6	5E+0.2	0.21	0.34	2.2E+02	3.5E+02	0.08	0.33
$Fiber4$	2.7	4.8E+02	0.20	0.32	2.1E+02	3.3E+02	0.07	0.28
$Fiber5$	2.4	4.3E+02	0.20	0.31	2.1E+02	3.2E+02	0.09	0.32
$Fiber6$	2.7	4.5E+02	0.20	0.36	2.1E+02	3.7E+02	0.07	0.38
$Fiber7$	2.4	4.4E+02	0.20	0.31	2.1E+02	3.2E+02	0.08	0.31
$Fiber8$	3.0	4.7E+02	0.21	0.31	2.2E+02	3.2E+02	0.08	0.28

y: yielding

f: fracture

In this study values for Fiber 8 from Table 4.1[6] are used since the modulus of hardening is equal to mean value and the other parameters vary in a small interval. The stress-strain curve for this material is shown in Figure 4.5. ABAQUS requires the true stress-strain curve for plastic material model [20]. Data set can be obtained by

using the following formulation;

$$\varepsilon = ln(1 + \varepsilon_{nom}) \tag{4.2}$$

$$\sigma = \sigma_{nom}(1 + \varepsilon_{nom}) \tag{4.3}$$

$$\varepsilon^{pl} = \varepsilon^{t} - \varepsilon^{el} = \varepsilon^{t} - \frac{\sigma}{E} \tag{4.4}$$

where ε^{t} is the total strain at the instant, ε^{pl} is the total plastic strain and ε^{el} is the total elastic strain.

In order to define plastic data, plastic behavior is interpolated linearly between yield point and fracture point. Engineering stress-strain values are converted to true stress-strain values are shown in Table 4.2 and Figure 4.6.

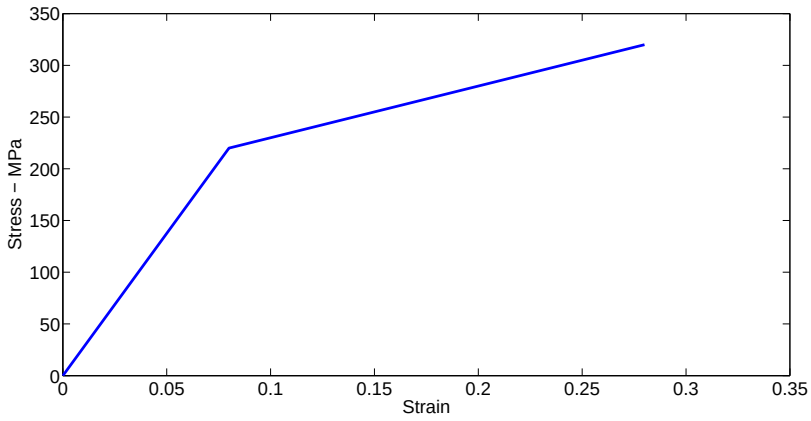

Figure 4.5. Related plasticity data - Nominal stress-strain curve used in analysis

Table 4.2. Converted Data for Fiber 8

Yield Stress(MPa)	Yield Strain
224.7	0
246.567	0.0113014
261.055	0.0227326
285.95	0.040961
303.067	0.0525568
321.487	0.0642668
343.101	0.0770796
365.313	0.0893
391.018	0.102358
417.481	0.114706
448.8	0.128032

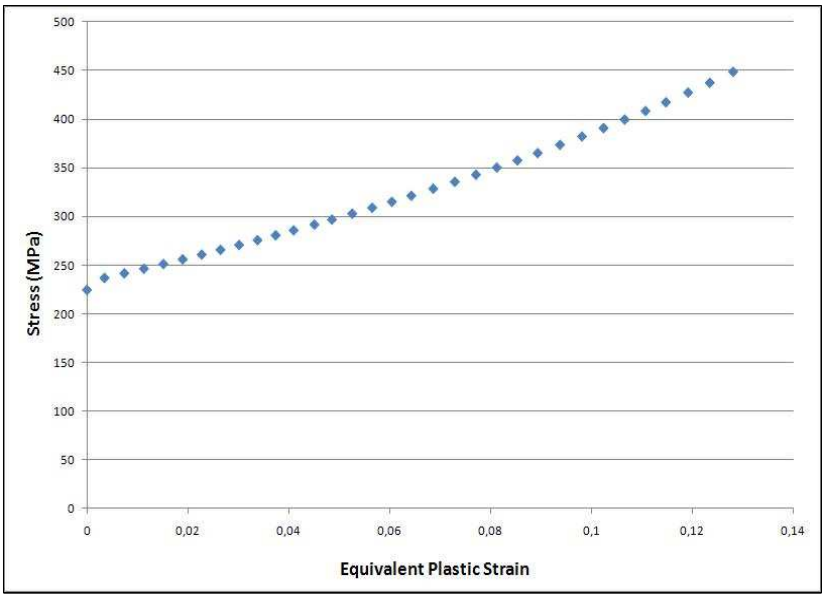

Figure 4.6. Real stress-strain curve for plastic part

The maximum value of coefficient of friction is taken as 0.4 which is the kinetic coefficient of fiber-on-fiber friction [21].

4.3. Mesh

Mesh consisted of linear brick elements C3D8 which are known to produce more accurate results than tetrahedrons. Some analyses were done using quadratic elements C3D20 to evaluate the effect of element type. Since the results did not change much, but the computing time increased significantly all analyses were done with linear elements.

In Model 1 both yarns have the same mesh with coinciding nodes on contact surface initially. Because brick elements have no rotational degree of freedom, constraint definitions are used in order to apply rotational displacements. Therefore nodes at the end surfaces of yarns are connected to reference points. Coinciding nodes at these surfaces are also constrained by contact definition. This situation causes over-constraint problem which directly affects the convergence in the step of twist of yarns. Therefore one of the parts was defined 0.1 mm longer than the other one. Two parts were assembled in such a way that end nodes of both parts did not coincide. Mesh of yarns becomes finer at the ends. There are 8932 elements in each yarn. Mesh was created as structured by using cell partition. Mesh of Model 1 is shown in Figure 4.7

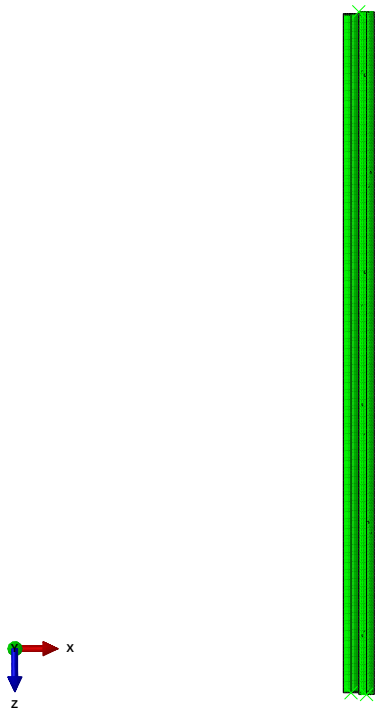

Figure 4.7. Model with modified ends - Mesh for Model 1

Second model in which twisted geometry is the initial configuration as seen in Figure 4.8, meshes could not be made structured. This is because partition could not be made due to helical geometry. In this model there are 9108 elements in each part. There is no modification at the ends of parts since there is no over-constraint problem.

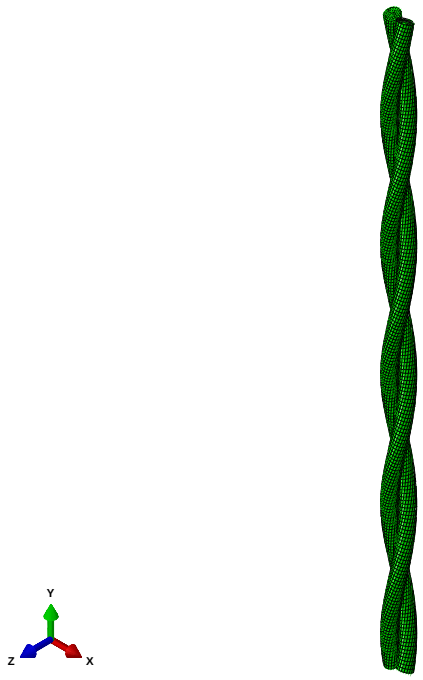

Figure 4.8. Twisted Geometry - Mesh for Model 2

4.4. Loading & Boundary Conditions

Three types of loadings were considered in the study:

- Twisting of each yarn
- Twisting yarns together
- Uniaxial tension of twisted yarns

In the models three different combinations of these loading types can be used. These are

- Twisting of each yarn → Twisting together → Tension

- Tension loading of twisted geometry
- Twisting together → Tension

The purpose of these combinations is to investigate the effect of loading applied in production process.

In order to twist separately or together, rotational displacement is defined at the ends. The nodes which are at the ends of the yarns are connected to reference points by using Rigid Body Constraint. Therefore rotational displacement is applied to reference nodes which have 6 degrees of freedom. For twisting separately one reference point is used for each yarn. For twisting together, on the other hand, one reference point is used for both yarns. For these two different loadings, constraints are applied at different ends. In other words for twisting separately constraints are defined at top surfaces whereas for twisting together constraint is defined at bottom surfaces.

Constraining the coinciding nodes by two different constraints causes over-constraint since contact formulation also applies constraints to these points. So the ends are shifted as mentioned in Section 4.1.

The twist level of the cord is determined with respect to the samples. The samples have 2.5 turn in 20 mm. Therefore rotational displacement for twisting yarns is 15.708 radians. Also rotational displacement for twisting of each yarn is taken as 15.708 radians which is equal to 900 degrees (2,5 turns). These values are same for all models where twisting is done. The only exception is for the analysis where General Contact is defined with Static-Kinetic Exponential Decay Friction. In this analysis the aim was to see how much yarns can be twisted together.

Due to convergence difficulties pre-tension loading is applied before twisting each yarn. On the contrary it is observed that there is no effect of pre-tension loading on convergence when twisting together.

Another important issue is constraining the yarns on z-axis. When a rotational displacement is applied, no constraint is applied about z-axis. So model is free to deform on z-direction. This directly improves convergence of problem. The deformations in other two directions (x-direction and y-direction) are constrained.

Tension loadings in final steps of analyses are done by defining a displacement boundary condition. The maximum amount of displacement for which converged so-

lution was obtained is 6.54 mm for Model 2 and 1.75 mm.

4.5. Contact Conditions

For contact surface properties, various types of behavior is used. These are;

- For normal behavior→ Hard Contact, Exponential Pressure-Overclosure
- For tangential behavior→ Frictionless, Penalty Friction, Static-Kinetic Exponential Decay friction

Tangential contact behavior is defined as frictionless in the step where yarns are twisted separately. For other loading types friction was defined through the following coefficients of friction:

- Penalty Friction with coefficient between →μ=0.01 and μ=0.4
- Static-Kinetic Exponential Decay Friction

Friction Coefficient^1	Slip Rate^1	Friction Coefficient^2	Slip Rate^2
0.25	0	0.4	0
0.1	2.5	0.2	2.5
0.1	Infinity	0.2	Infinity

The superscripts 1 and 2 represent two different set of coefficients are used for exponentially decaying friction.
The Parameters for Exponential Pressure Over-closure are taken as

Pressure (Pa)	Clearance (mm)
4.5E+06	0
0	1.75E-08

Both General and Surface-to-Surface contact options were used in the analysis. The former aims to facilitate modeling of contact and according to ABAQUS [20] it uses surface-to-surface formulation. Differences as predicted in the results are presented in Chapter 5.

4.6. Summary of Models

4.6.1. Model 1

The model consists of two yarns. Each yarn is meshed with 8932 linear elements. The length of two yarns differs by a small amount.
Three loading steps are defined for this model. Loadings are applied through reference points. These reference points are tied to ends of yarns by Rigid Body Constraint. In order to prevent over-constraint, one yarn is taken 0.1 mm longer than the other one.
Step 1: Pre-Tension loading of 5 N. (Step Time: 0-2) → Separately Twist of Yarns (Step Time: 1-2)

- Two reference points are used.
    i. These reference points are at z=20 (left ends of yarns). The rotational displacement is 15.708 radians which is equal to 2.5 turns.

Step 2: Twisting Yarns together (Step Time: 0-2)

- One reference point is used.
    i. This one is at z=0 (at the origin). The rotational displacement in Step 2 is also 15.708 radians which is equal to 2.5 turns.

Step 3: Tension loading of Rope (Step Time: 0-2)

- Tension loading is applied by using the same reference point used in Step 2. Tension is applied as displacement. Currently there is no limit for tension loading from convergence point of view. Model is still being enforced in order to converge its possible maximum state.

Contact condition is defined on side surfaces by extracting end regions of yarns. Used tangential behavior is Penalty Friction and Static-Kinetic Exponential Decay Friction. Surface to Surface Contact and General Contact were tried for this model.

4.6.2. Model 2

In this model the initial geometry is the twisted rope. This geometry is obtained by using revolution tool. There are two parameters for creating the geometry. First parameter is the angle which defines the total twist level of yarn. Second parameter is the pitch, length in which geometry completes a revolution. The values of these parameters are;
Angle: 900(in degrees)
Pitch: 8 (mm.)

- Meshes are identical for both yarns. However meshes are not structured as in the other models because part could not be partitioned. There are 9108 elements in each part.
- There is only one step defined in this model. That is the tension loading of rope.
- In this model there is only one constraint definition (Rigid Body Constraint) since there is no twist (or rotational loading). Tension loading is applied by using a reference point (which is tied to yarns at their ends).
- Contact condition is defined on side surfaces by extracting end regions of yarns. Used tangential behavior was Penalty Fiction. Surface to Surface Contact was defined in this model.

4.6.3. Other Models

In order to see the effect of initial twist of yarns on the uniaxial tension of rope, a third model was analyzed. This model has the same geometry, mesh, contact properties as Model 1. However different from Model 1 there is no initial twist and no initial tension loading (i.e. Step 1 is discarded). The first step of loading is twisting yarns together. Since model has not been satisfactorily converged tension loading has not been applied.

Different contact formulations have no significant effect on convergence of Model 2. Therefore the results of Model 2 is given only for the penalty method.

5. RESULTS

The analysis results of FE models described in Chapter 4 are presented in the following.

First deformed configurations and contact surfaces are discussed. Second, load-displacement curves are given and the effect of various parameters on the plots are discussed. Finally, comparison with analytical solution is presented.

5.1. Deformed Configurations

Figures 5.1 and 5.2 show deformed configurations at the end of tension loading for Model 1 and Model 2, respectively. The pitch length of rope is varying along the yarn axis in Model 1 whereas it is constant in Model 2. This variation in Model 1 is because of the propagation of twist from one end to the other.

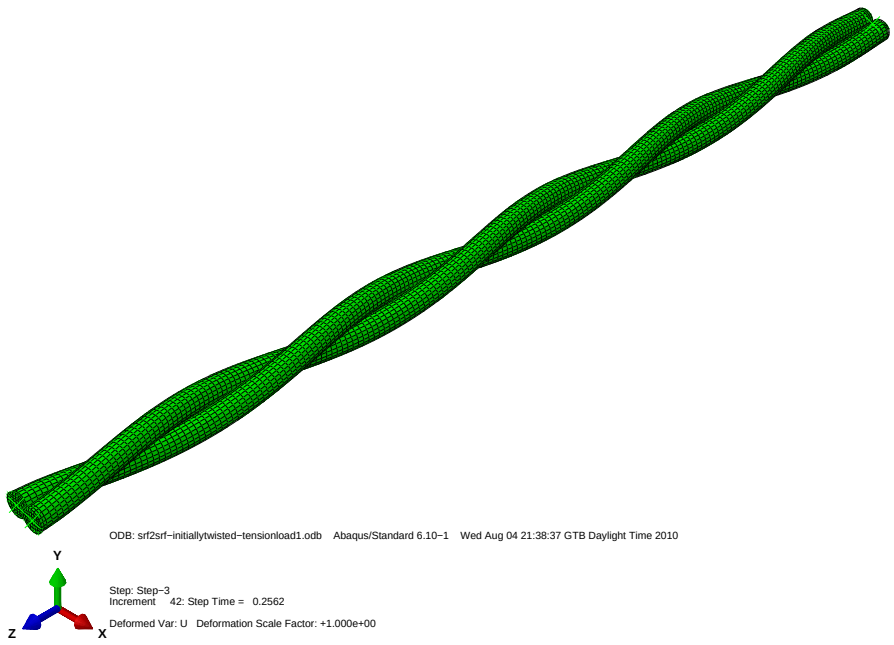

Figure 5.1. Deformed geometry for 1.31 mm axial displacement - Model 1

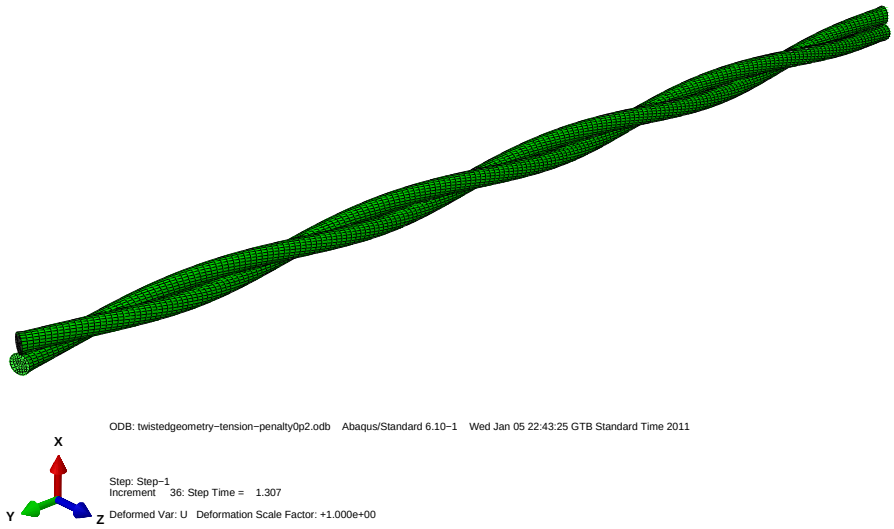

Figure 5.2. Deformed geometry for 6.53 mm axial displacement - Model 2

Figures 5.3 to 5.6 compare contact pressure distributions using General and Surface to Surface contact options for Model 1.

The expected contact surfaces are as suggested by Hertz theory [17], that is elliptical after twist of yarns and stripe or narrow rectangle after tension loading. This expectation is fulfilled in both General contact and Surface-to-Surface Contact models. However, comparison shows difference in contact pressure distribution and maximum values. This may be due to differences in contact algorithms or their implementation. For example automatic detection and removal of overconstraints in General Contact algorithm may lead to decreased number of nodal constraints.

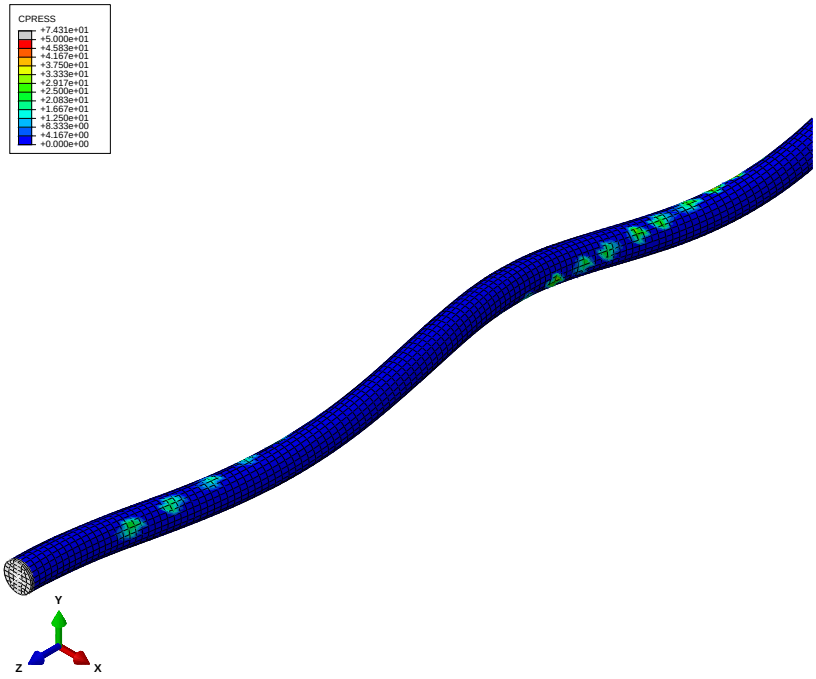

Figure 5.3. Contact pressure distribution after twist of yarns - General Contact

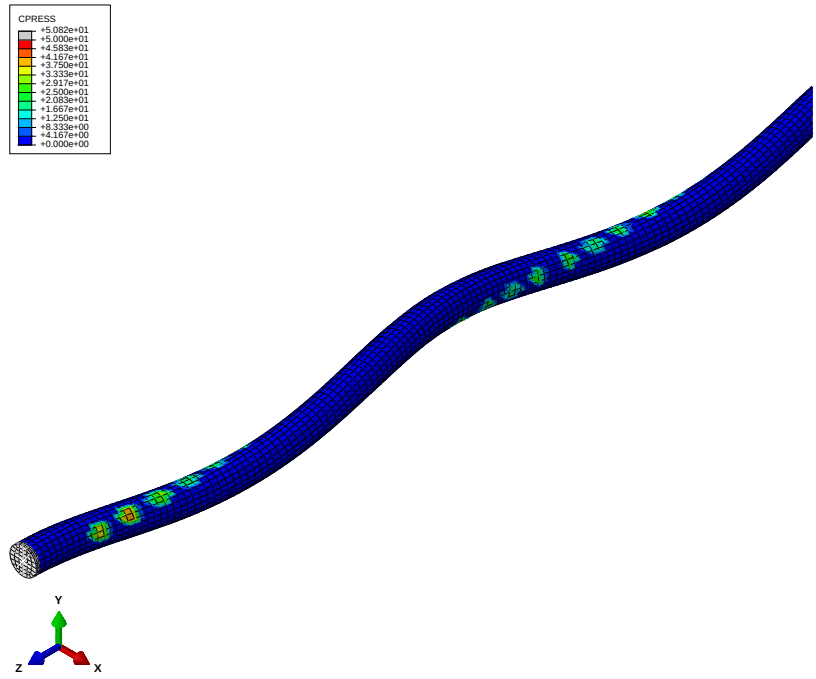

Figure 5.4. Contact pressure distribution after twist of yarns - Surface to Surface Contact

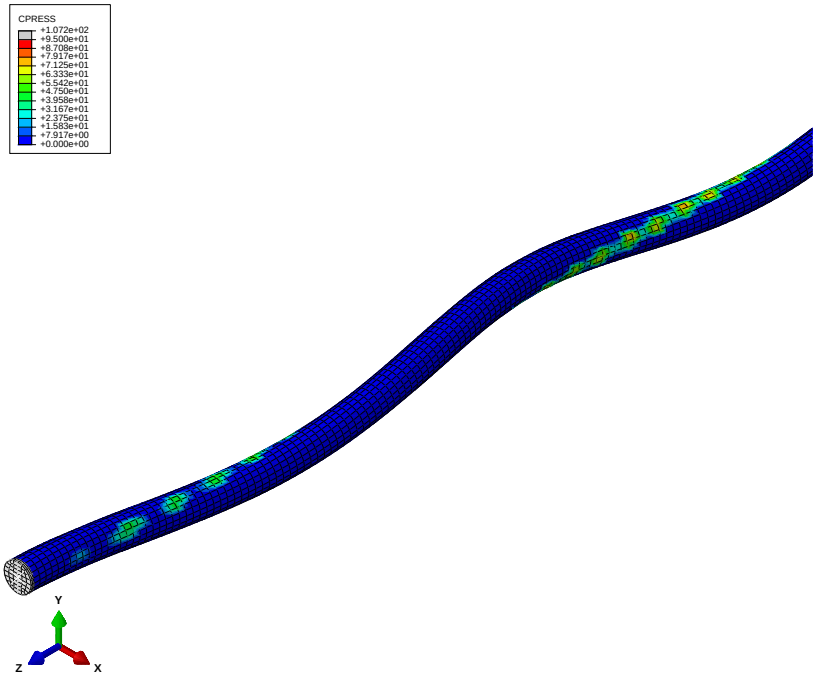

Figure 5.5. Contact pressure distribution after tension loading - General Contact

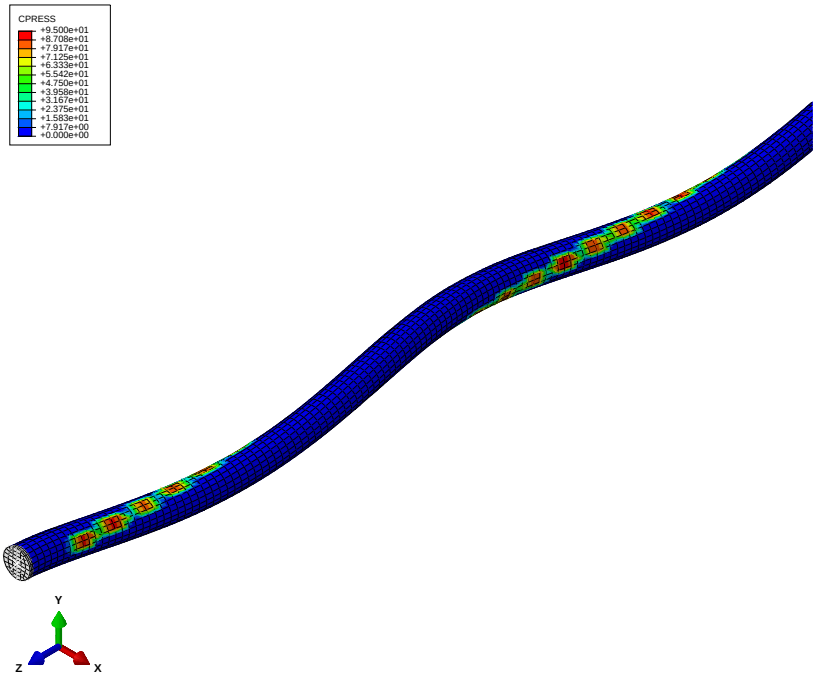

Figure 5.6. Contact pressure distribution after tension loading - Surface to Surface Contact

The contact area after tension loading is a narrow rectangle for Model 2 as it is predicted by Hertz theory. Contact surface for Model 2 is shown in Figure 5.7.

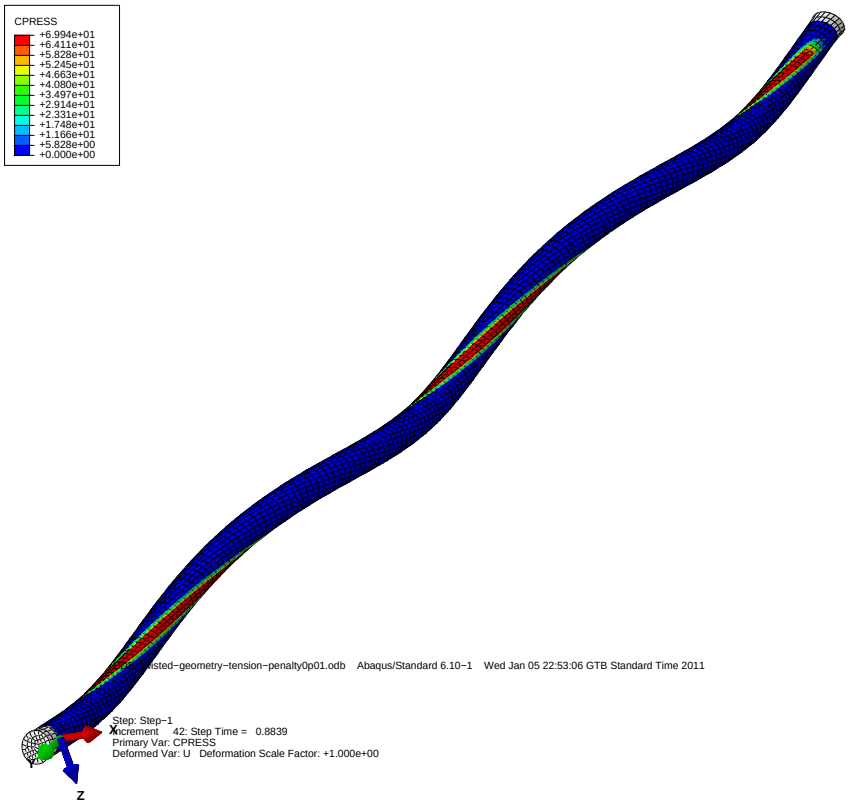

Figure 5.7. Contact surface after tension loading - Model 2

The contact pressure variation along the contact line are shown in Figure 5.8 and 5.9 for Model 1 and Model 2 respectively.

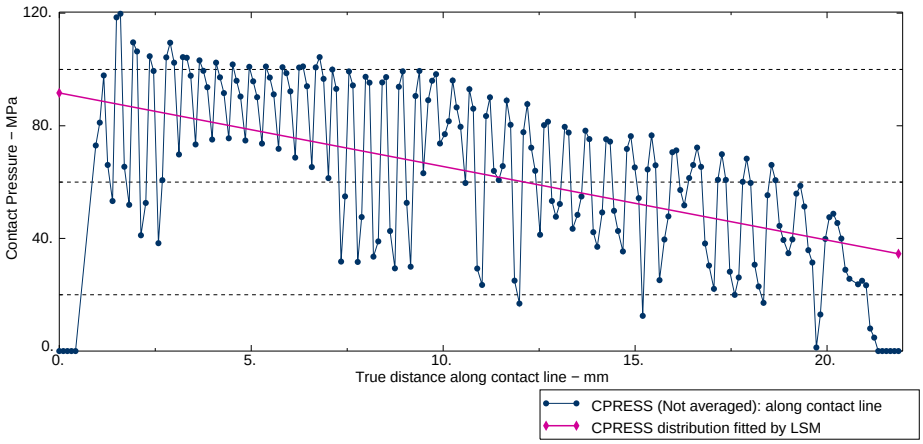

Figure 5.8. Contact pressure along the contact line for Model 1

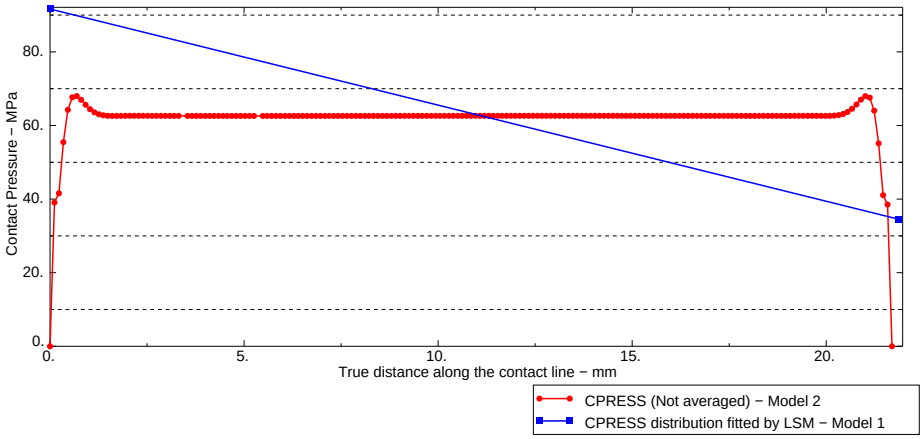

Figure 5.9. Contact pressure along the contact line for same axial displacement

The Mises Stress values are consistent with contact pressure for Model 1 on the contact surface. Variation of Mises Stress along the contact line is shown in figure 5.10;

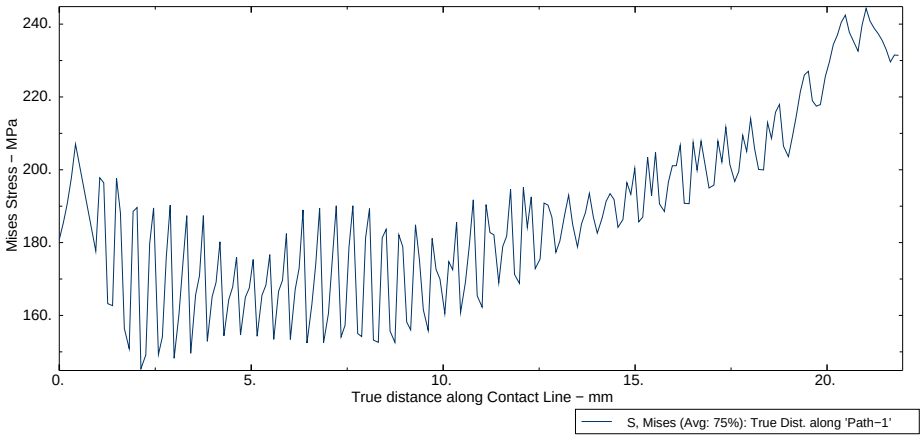

Figure 5.10. Mises stress along the contact line for 1.3 mm. axial displacement - Model 1 σ_y=220 MPa

The stress distribution on the cross section agrees well with that predicted by Hertzian theory. The stress distribution on the cross section of rope is shown in Figure 5.11.

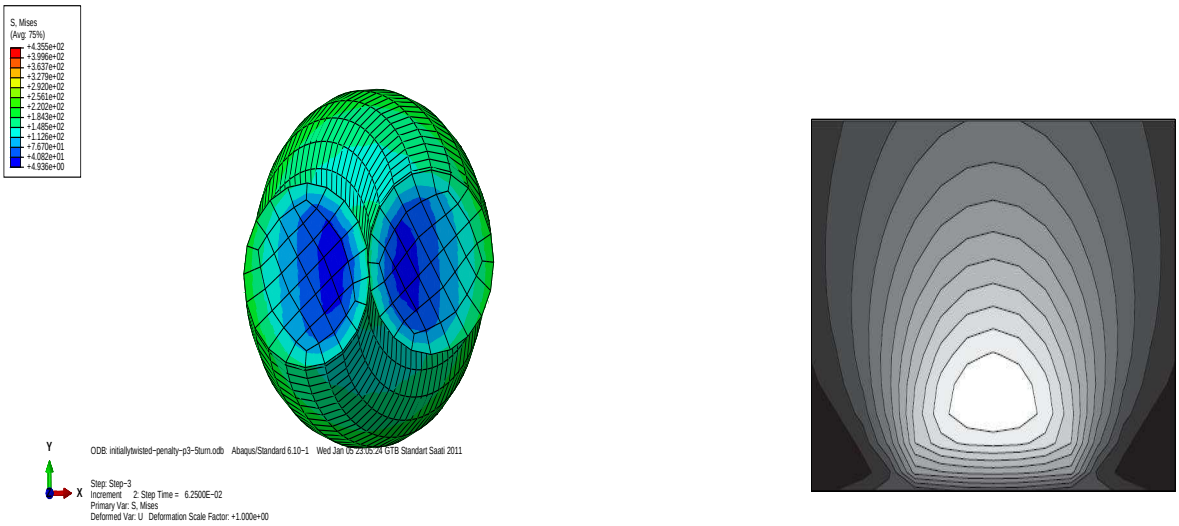

(a) Model 1 (b) Hertz theory [18]

Figure 5.11. Stress distribution on cross section

The Mises stress values predicted by Model 1 are higher than the values predicted by Model 2. Therefore the effect of initial loadings is significant. Maximum Mises stress values occur in outer surface of rope structure for Model 1 whereas they occur on the contact surface for Model 2. The stress distributions on the same cross-section for the same displacement are shown in Figure 5.12 and 5.13 for Model 1 and Model 2 respectively.

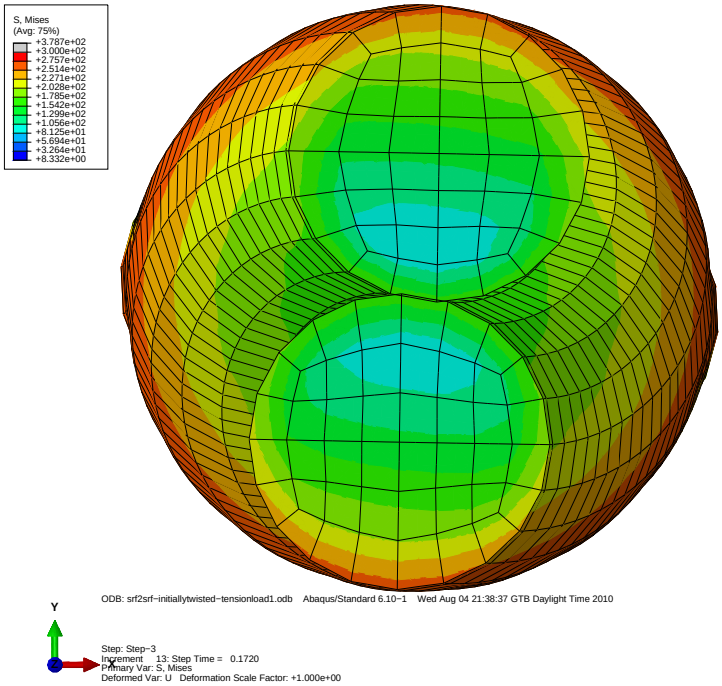

Figure 5.12. Mises stress distribution for axial displacement$\simeq$ 0.87 mm - Model 1 σ_y=220 MPa

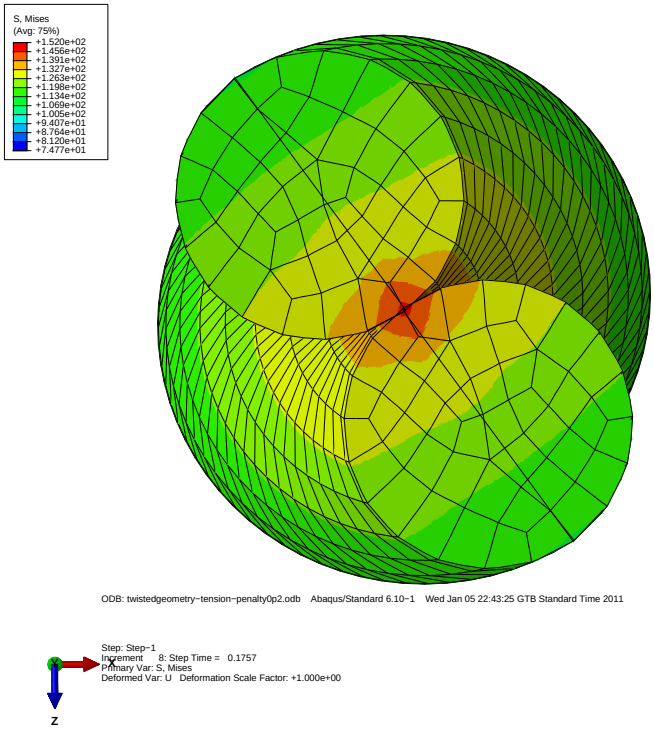

Figure 5.13. Mises stress distribution for axial displacement$\simeq$ 0.87 mm - Model 2 σ_y=220 MPa

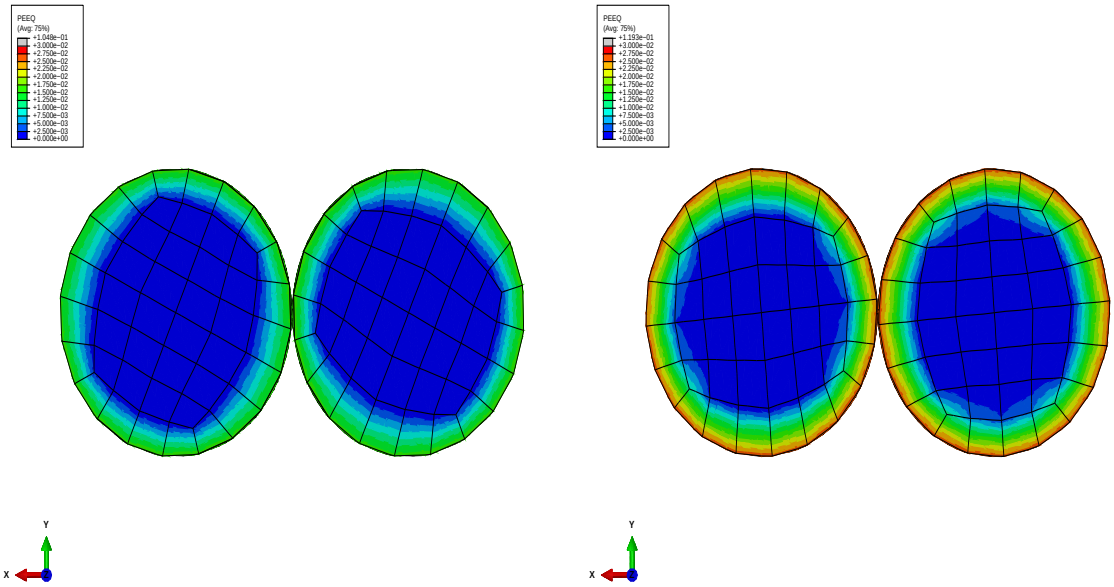

(a) at 13.11 radians

(b) at 14.78 radians

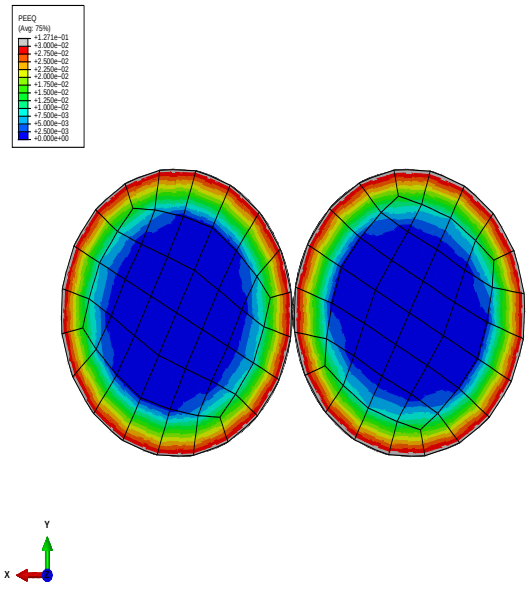

(c) at 15.70 radians

Figure 5.14. Plastic strain distribution on cross section for Model 1 - Step 1

Initial twisting and twisting of yarns cause hardening. Plastic strain is observed in these steps. Twisting of yarns causes axial contraction. Therefore pitch length changes during twisting of yarns. Plastic strain values at various loading steps are shown in Figures 5.14, 5.15, 5.16 and 5.17.

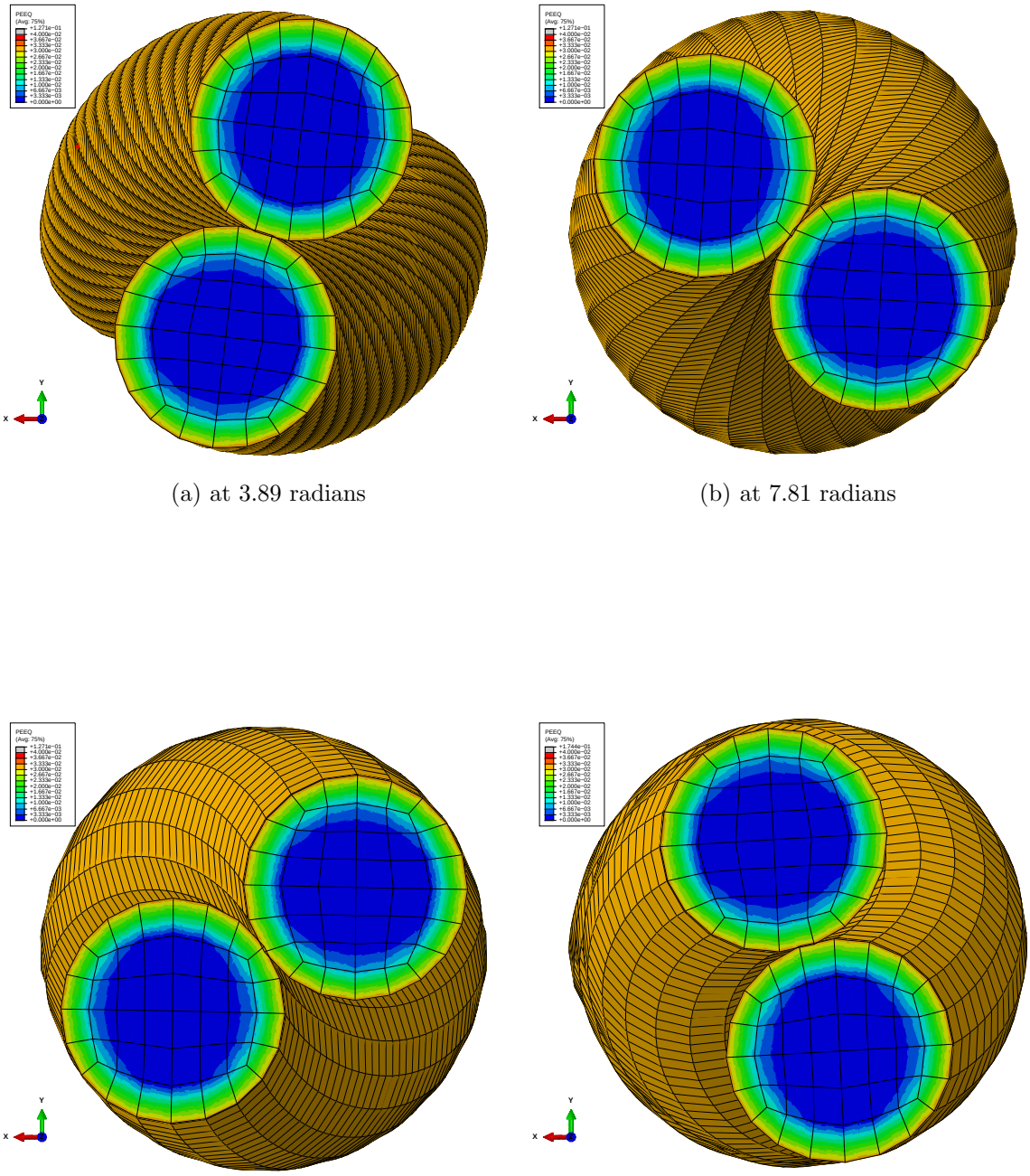

(a) at 3.89 radians

(b) at 7.81 radians

(c) at 11.75 radians

(d) at 15.70 radians

Figure 5.15. Plastic strain distribution on cross section for Model 1 - Step 2

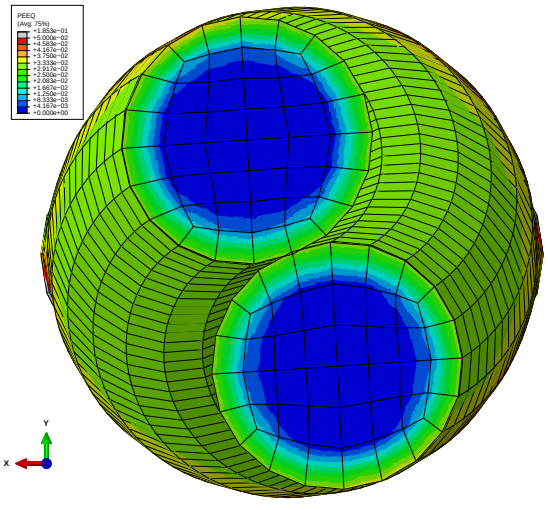

(a) Model 1 at 0.98 mm. axial displacement

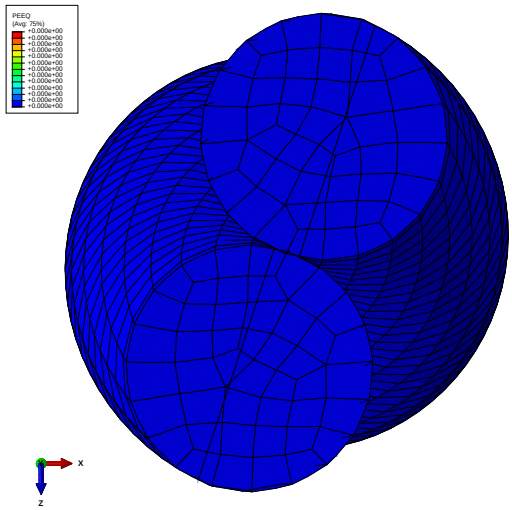

(b) Model 2 at 0.98 mm. axial displacement

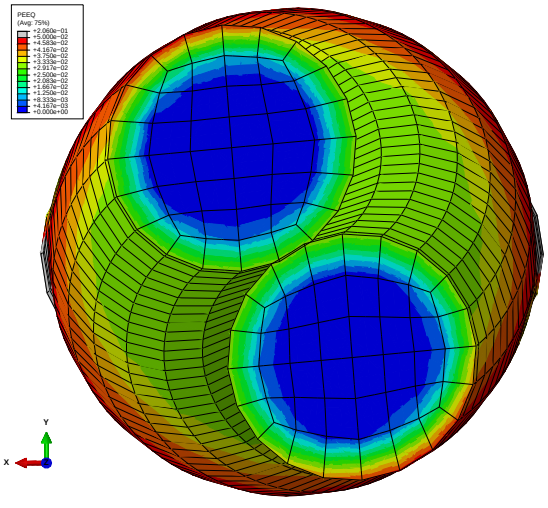

(c) Model 1 at 1.32 mm. axial displacement

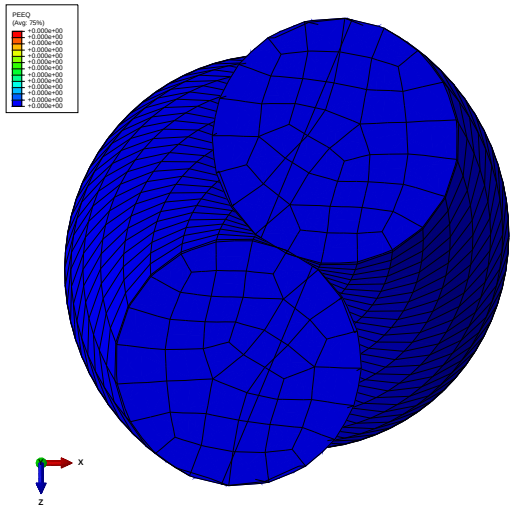

(d) Model 2 at 1.32 mm. axial displacement

Figure 5.16. Plastic strain distribution on cross section for Model 1 and Model 2

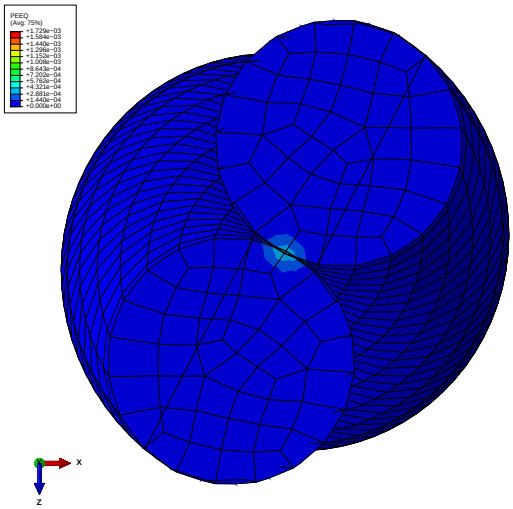

(a) at 1.40 mm. axial displacement

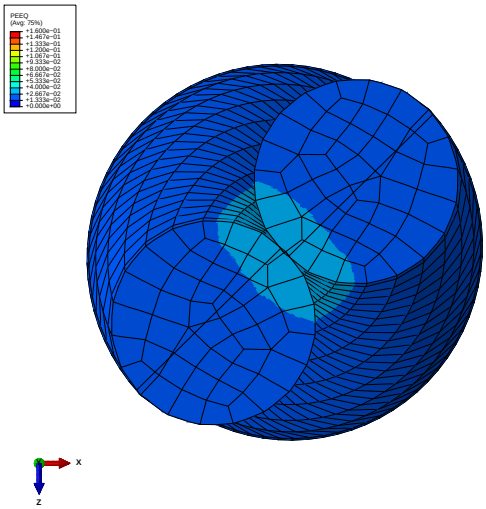

(b) at 2.41 mm. axial displacement

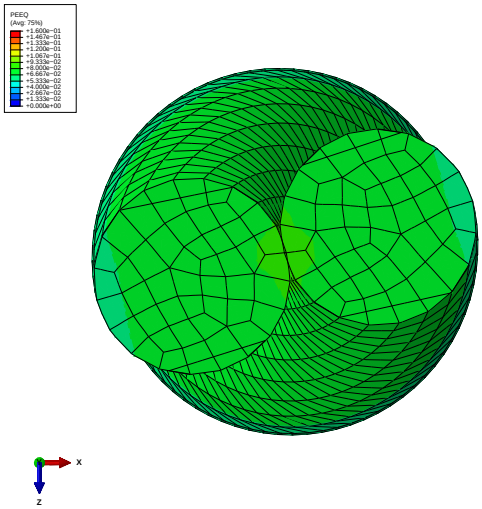

(c) at 4.19 mm. axial displacement

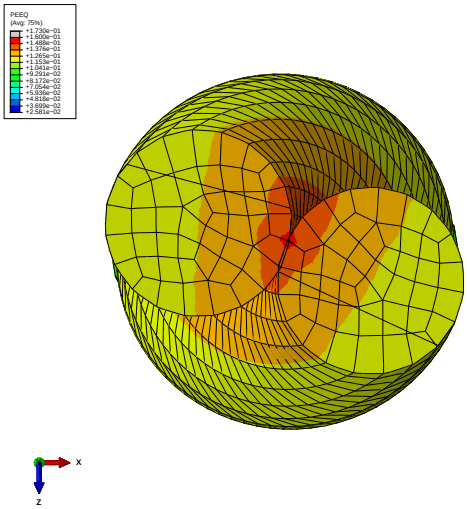

(d) at 6.54 mm. axial displacement

Figure 5.17. Plastic strain distribution on cross section for Model 2

The contact pressure variation along contact line for various twist levels is shown in Figure 5.18.

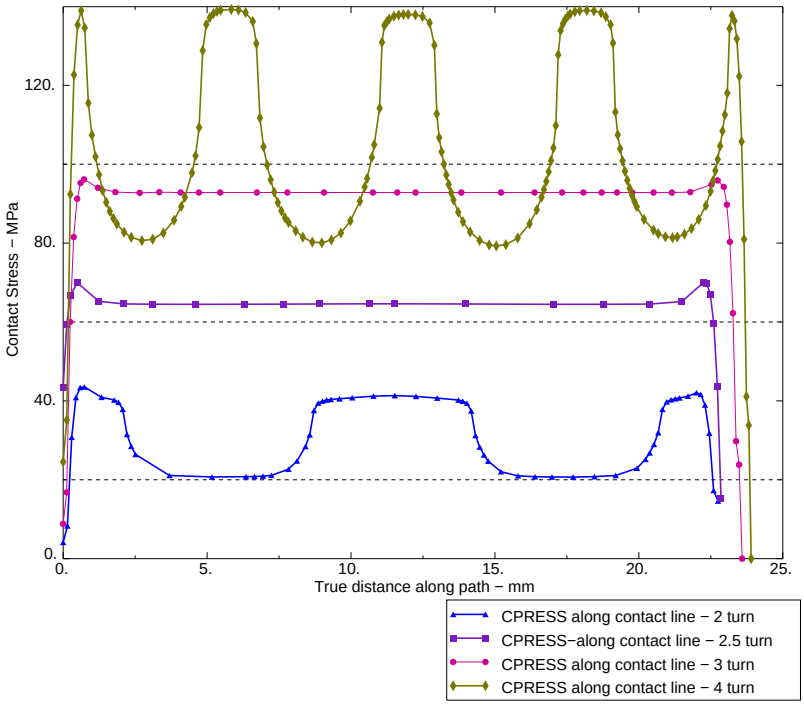

Figure 5.18. Position vs contact pressure along the contact line for 4 mm. displacement - Model 2

The contact stresses increase with increasing twist level. Based on Figure 2.4 it can be concluded that Costello's analytical calculation of contact pressure will give much higher values as compared to finite element prediction.

5.2. Axial Response

The load-displacement curves for Model 1 and Model 2 are compared in Figure 5.19. For Model 1 both General Contact and Surface to Surface Contact results are shown. It is also observed that twist of yarns in Model 1 causes contraction in the axial direction. Since Model 2 has converged for greater displacements and since the slope of the curves are same in Model 1 and Model 2, Model 2 was used to study the effect of various parameters on the axial response. The results of Model 2 with penalty method is given.

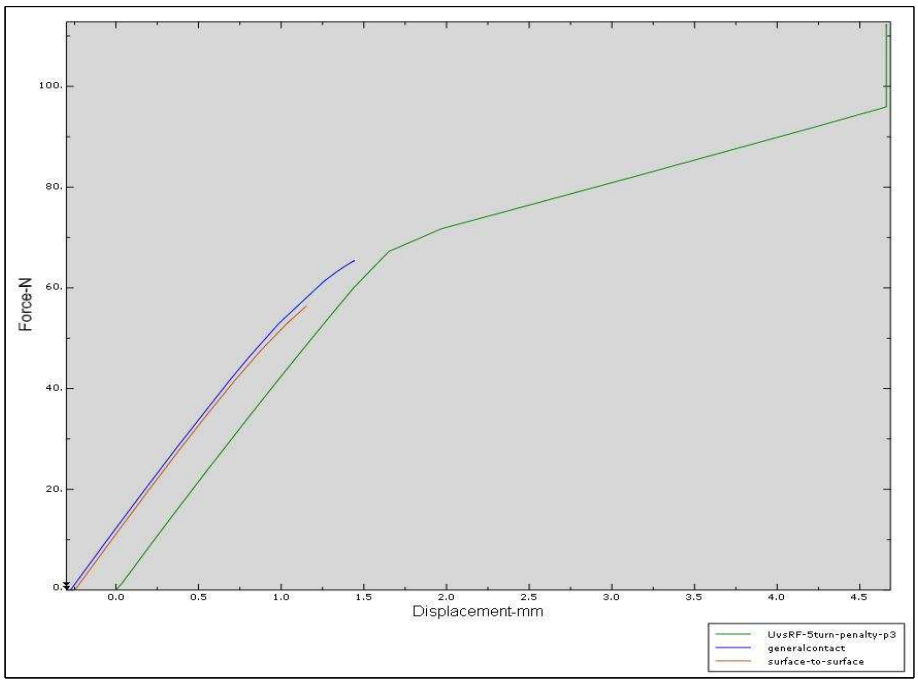

Figure 5.19. Comparison of convergence

As the twist level decreases the axial response of cord becomes stiffer. Therefore twist level changes the stiffness of cord structure.

For different twist levels the effect of friction was also investigated. Results are shown in Figures 5.21 - 5.24. Insignificant effect of friction on axial response was observed. The only effect of friction was observed on the solution. As seen in Figure 5.21, higher friction coefficient gave a smoother force-displacement curve. No effect of friction was observed on the smoothness for other twist levels.

The effect of twist level on the response of two ply cord is shown in Figure 5.20. Twist level has significant effect on the axial response of the rope. As the twist level increases, stiffness of the cord decreases.

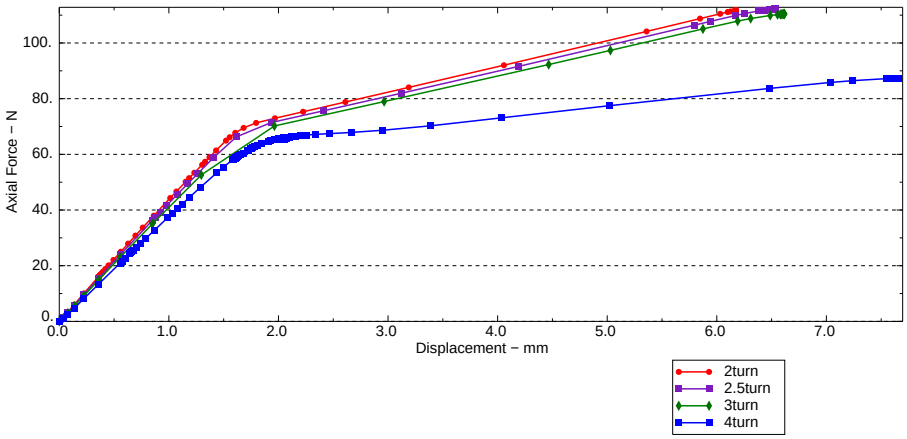

Figure 5.20. Load-Displacement curve for various twist rates

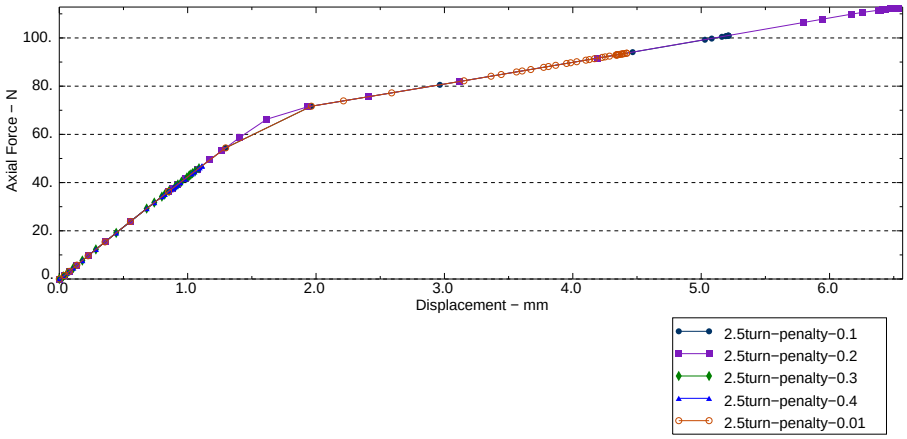

Figure 5.21. Load-Displacement curve for 2.5-turn Model 2 with various friction

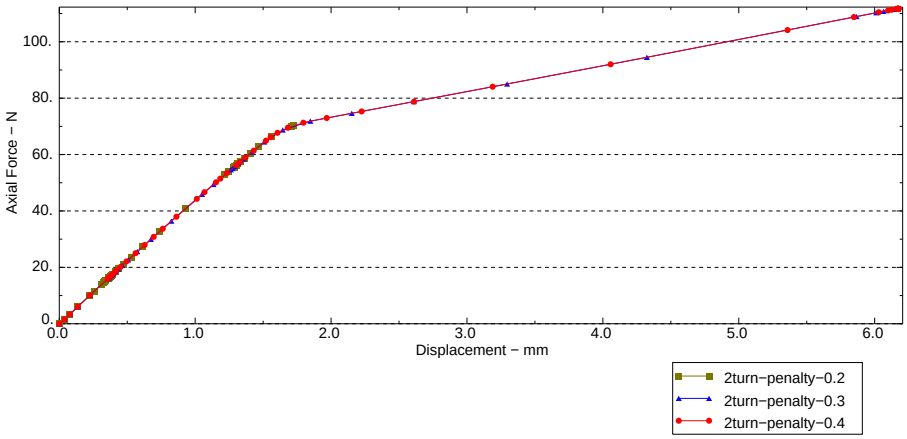

Figure 5.22. Load-Displacement curve for 2-turn Model 2 with various friction coefficients

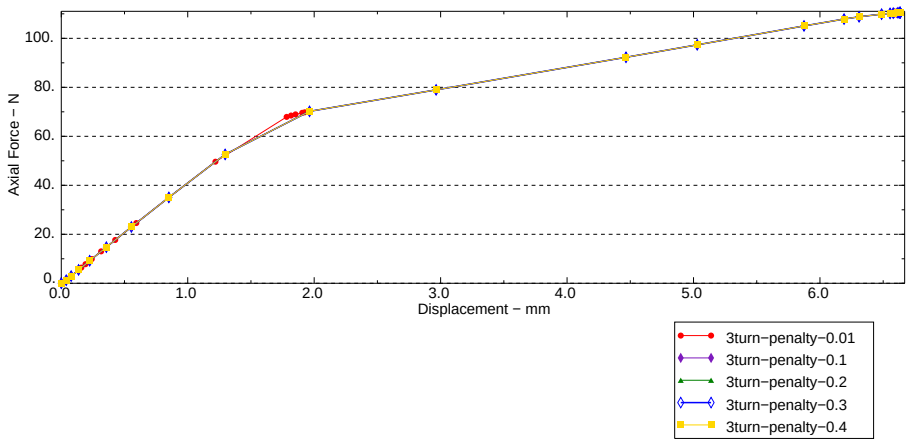

Figure 5.23. Load-Displacement curve for 3-turn Model 2 with various friction coefficients

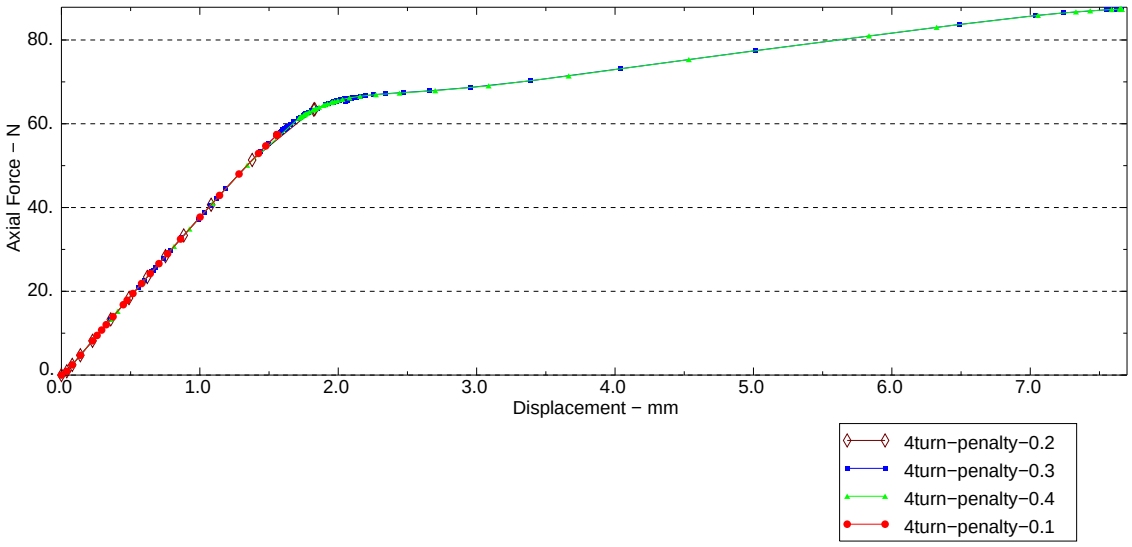

Figure 5.24. Load-Displacement curve for 4-turn Model 2 with various friction coefficients

5.3. Comparison of Predictions and Analytical Solution

The axial response of Model 2 and analytical solution proposed by Costello [15] are shown in Figures 5.25-5.28. It is observed that in the elastic region predictions and analytical results based on small strain theory and linear elastic behavior are in agreement.

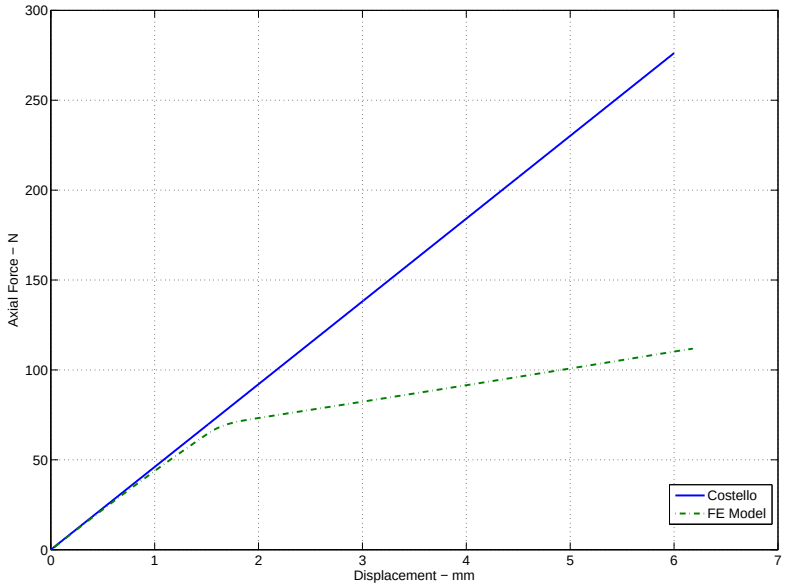

Figure 5.25. Load-Displacement curve - Comparison for analytical results and FEA results - 2 turn

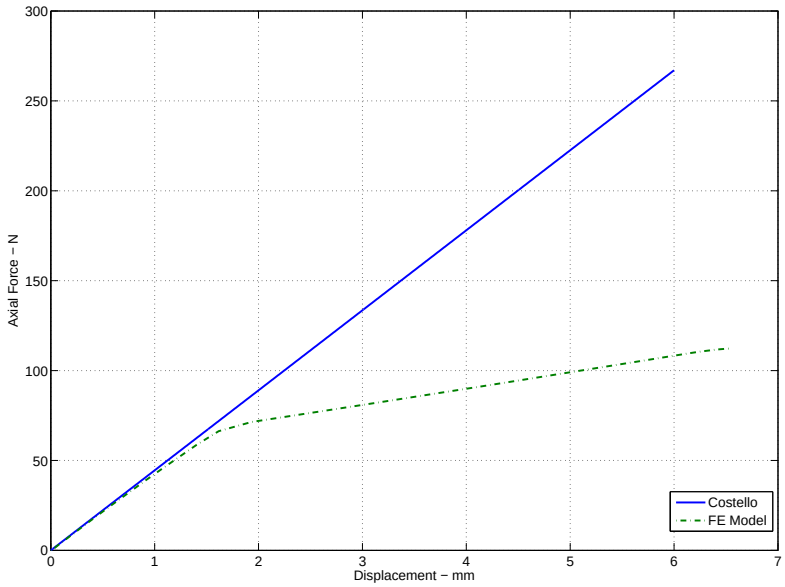

Figure 5.26. Load-Displacement curve - Comparison for analytical results and FEA results - 2.5 turn

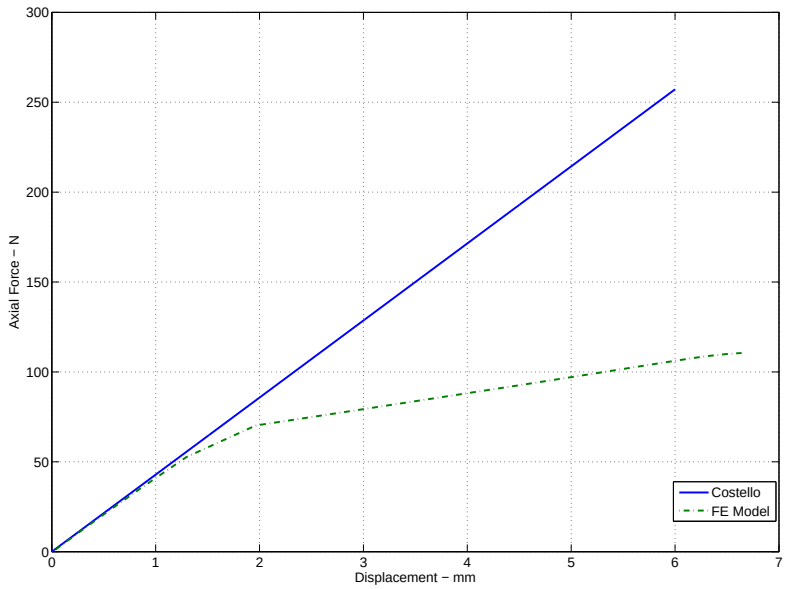

Figure 5.27. Load-Displacement curve - Comparison for analytical Results and FEA results - 3 turn

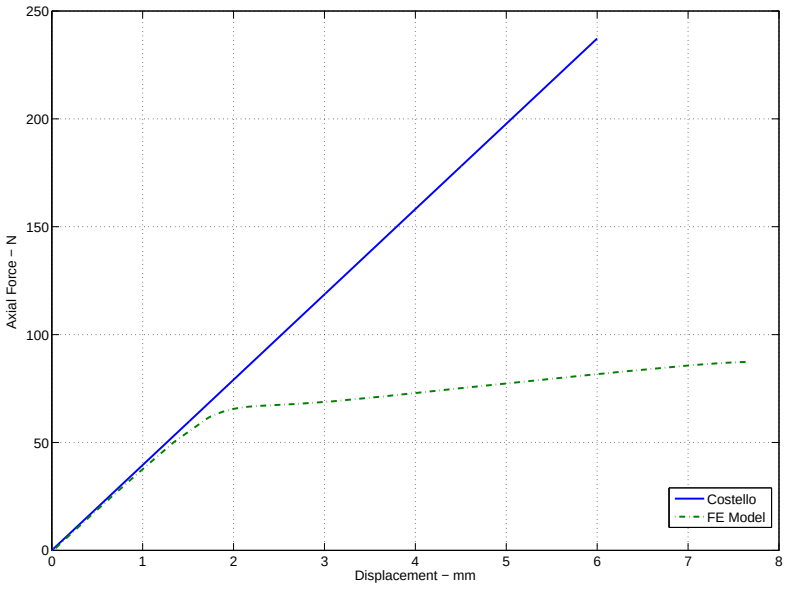

Figure 5.28. Load-Displacement curve - Comparison for analytical results and FEA results - 4 turn

6. CONCLUSIONS

In this study computational models for twisted yarns and ropes that are composed of many synthetic fibers are developed.Various contact models and the effect of various parameters on mechanical behavior of rope are investigated. Formulations available in the literature are investigated and results of these formulations are compared with the finite element results.

Modeling yarn twist has negligible effect on the overall response, that is load displacement relation, of the rope. On the other hand significant effects are predicted for stress values.

Convergence difficulties are mainly due to contact. Presence of plastic deformations increases the level of difficulty. Both Lagrange multiplier method and penalty method give similar analysis results. First choice will be the penalty method for further analyses since it generally reduces the number of iterations required.

Initial twisting and twisting of yarns cause hardening. Plastic strain is observed in these steps. Twisting of yarns causes axial contraction. Therefore pitch length changes in twisting of yarns.

Twist level has significant effect on the axial response of the rope. As the twist level increases, stiffness of the cord decreases. Variation of friction coefficient has insignificant effect on the overall response.

Overall response agrees with the analytical solution based on small strain theory and linear elastic behavior.

Experimental data is essential for a complete verification of the current model and analysis results.

Future work would include evaluation of viscoelastic behavior of yarns. Modeling of individual fibers and the interaction among them could also be considered.

REFERENCES

1. Zimliki, D. A., J. M. Kennedy, and D. E. Hirt, "Determining Mechanical Properties of Yarns and Two-Ply Cords from Single-Filament Data: Part I: Model Development and Predictions", *Textile Research Journal* 70:11, pp. 991-1004, 2000.

2. Leech, C. M., "The modelling of friction in polymer fibre ropes", *International Journal of Mechanical Sciences* 44, pp. 621-643, 2002.

3. Chailleux, E. and P. Davies, "Modelling the Non-Linear Viscoelastic and Viscoplastic Behaviour of Aramid Fibre Yarns", *Mechanics of Time-Dependent Materials* 7, pp. 291-303, 2003.

4. Chailleux, E. and P. Davies, "A Non-Linear Viscoelastic Viscoplastic Model for the Behaviour of Polyester Fibres", *Mechanics of Time-Dependent Materials* 9, pp. 147-160, 2005.

5. Adolf, D. B., R. S. Chambers, D. C. Hammerand, M-Y. Tang , K. Westgate, J. Gillick, and I. Skrypnyk, "Modeling the response of monofilament nylon cords with the nonlinear viscoelastic, simplified energy clock model", *Polymer* 51, pp. 1530-1539, 2010.

6. Averett, R. D., M. L. Realff, S. Michielsen, and R. W. Neu, "Mechanical behavior of nylon 66 fibers under monotonic and cyclic loading", *Composites Science and Technology* 66, pp. 1671-1681, 2005.

7. Lunn, A. C., B-L. Lee, and I. V. Yannas, "Strain Recovery of Polyester and Nylon 66 Monofilaments under Various Temperature Histories", *Polymer Engineering and Science* 14:9, pp. 610-615, 1974.

8. Blanc, R. A. and A. Ravasoo, "On the Nonlinear Viscoelastic Behaviour of Nylon Fiber", *Mechanics of Materials* 22, pp. 301-310, 1996.

9. Padovan, J., "Thermoelasticity of Unidirectionally Micropolar Cord-Reinforced Composites", *Journal of Thermal Stresses* 18:3, pp. 383-401, 1995.

10. Padovan, J., "Thermoelastic Load Transfer Between Twisted Cord and Matrix in Composites", *Journal of Thermal Stresses* 18:5, pp. 551-571, 1995.

11. Pidaparti, R. M. V. and A. W. May, "A micromechanical analysis to predict cord-rubber composite properties", *Composite Structures* 34, pp. 361-369, 1996.

12. Pidaparti, R. M., S. Jayanti, J. Henkle, and H. El-Mounayri, "Design simulation of cord-rubber structure using PorE/ANSYS", *Composite Structures* 52, pp. 287-294, 2001.

13. Yeoh, O.H., "Some benchmark problems for FEA from torsional behavior of rubber", *Rubber Chemistry and Technology* 76:5, pp. 1212-1227, 2003.

14. Leech, C. M., "Theory and numerical methods for the modeling of synthetic ropes", *Communications in Applied Numerical Methods*, 3, pp. 407-413, 1987.

15. Costello, G. A., *Theory of Wire Rope*, 2nd ed., Springer, New York, pp. 37-39, 1997.

16. Boresi, A. P. and O. M. Sidebottom, *Advanced Mechanics of Materials*, 4th ed., Wiley, New York, pp. 629-631, 1985.

17. Johnson, K.L., *Contact Mechanics*, Cambridge University Press, Cambridge, pp. 84-101, 1987.

18. Popov, V. L., *Contact Mechanics and Friction, Physical Principles and Applications*, Springer-Verlag, Berlin, pp. 55-67, 2010.

19. Wriggers, P., *Computational Contact Mechanics*, J. Wiley and Sons Ltd., Chichester, 2002.

20. ABAQUS 6.10 Documentation, SIMULIA Inc. 2010.

21. Warner, S.B., *Fiber Science*, Prentice Hall Inc., New Jersey, pp. 248-249, 1995.